

The Origin of Intra-plate Ocean Island Basalts (OIB): the Lid Effect and its Geodynamic Implications

YAOLING NIU^{1,2*}, MARJORIE WILSON³, EMMA R. HUMPHREYS⁴
AND MICHAEL J. O'HARA⁵

¹SCHOOL OF EARTH SCIENCES, LANZHOU UNIVERSITY, LANZHOU 730000, CHINA

²DEPARTMENT OF EARTH SCIENCES, DURHAM UNIVERSITY, DURHAM DH1 3LE, UK

³SCHOOL OF EARTH AND ENVIRONMENT, THE UNIVERSITY OF LEEDS, LEEDS LS2 9JT, UK

⁴DEPARTMENT OF EARTH SCIENCES, UNIVERSITY OF BRISTOL, BRISTOL BS8 1RJ, UK

⁵INSTITUTE OF GEOGRAPHY AND EARTH SCIENCES, ABERYSTWYTH UNIVERSITY, ABERYSTWYTH SY23 3DB, UK

RECEIVED JUNE 30, 2010; ACCEPTED MAY 19, 2011

Based on an evaluation of major and trace element data for ocean island basalts (OIB), we demonstrate that oceanic lithosphere thickness variation, which we refer to as the lid effect, exerts the primary control on OIB geochemistry on a global scale. The lid effect caps the final depth (pressure) of melting or melt equilibration. OIB erupted on thick lithosphere have geochemical characteristics consistent with a low extent and high pressure of partial melting, whereas those erupted on thin lithosphere exhibit the reverse; that is, a high extent and low pressure of melting cessation. This observation requires that mantle melting beneath intra-plate volcanic islands takes place in the asthenosphere and results from dynamic upwelling and decompression. Melting beneath all ocean islands begins in the garnet peridotite facies, imparting the familiar 'garnet signature' to all OIB melts (e.g. $[Sm/Yb]_N > 1$); however, the intensity of this signature decreases with increasing extent of melting beneath thinner lithospheric lids as a result of dilution. The dilution effect is also recorded in the radiogenic isotope composition of OIB, consistent with the notion that their mantle source regions are heterogeneous with an enriched component of lower solidus temperature dispersed in a more refractory matrix. High-quality data on the compositions of olivine phenocrysts from mid-ocean ridge basalt and global OIB sample suites are wholly consistent with the lid effect without the need to invoke olivine-free pyroxenite as a major source component for OIB. Caution is necessary when using basalt-based thermobarometry approaches to estimate mantle potential temperatures and

solidus depth because OIB do not unequivocally record such information. For plate ages up to ~ 80 Ma, we demonstrate that the geophysically defined base of the growing oceanic lithosphere corresponds to both an isotherm ($\sim 1100^\circ\text{C}$) and the pargasite (amphibole) dehydration solidus of fertile mantle peridotite. As pargasite in $\text{H}_2\text{O}-\text{CO}_2$ -bearing mantle peridotite is stable under conditions of $T \leq 1100^\circ\text{C}$ and $P \leq 3$ GPa (~ 90 km), this solidus is essentially isothermal (i.e. $dT/dP \sim 0$ in P–T space) with $T \sim 1100^\circ\text{C}$ at depths ≤ 90 km, but becomes isobaric (i.e. $dP/dT \sim 0$ in P–T space) at the ~ 90 km depth. The latter explains why older (>70 Ma) oceanic lithosphere cannot be thicker than ~ 90 km without the need to invoke physically complex processes such as convective removal.

KEY WORDS: intra-plate volcanic islands; ocean island basalts; OIB chemistry; lithosphere thickness control; lid effect; dynamic upwelling; mantle plumes

INTRODUCTION

Plate tectonics theory readily explains why there is magmatism both at ocean ridges and along subduction zones and why the geochemistry of basalts from these two tectonic settings differs as a result of different processes operating

*Corresponding author. Present address: Department of Earth Sciences, Durham University, Durham DH1 3LE, UK.
Telephone: +44-19-1334-2311. Fax: +44-19-1334-2301.
E-mail: Yaoling.Niu@durham.ac.uk

at these two types of plate boundary. However, it cannot readily explain the widespread basaltic volcanism occurring in the interiors of tectonic plates (e.g. the age-progressive Hawaii–Emperor seamount chain in the Pacific; Wilson, 1963*a*, 1963*b*), leading to models for such within-plate volcanic centres that require mantle upwellings or plumes from a relatively fixed source in the mantle deeper than, and thus unaffected by, the moving tectonic plate. Early on in the debate, it was proposed that ‘hot-spots’ are the surface expressions of mantle plumes upwelling from the lowest part of the mantle, containing relatively primordial materials geochemically more enriched than the asthenospheric source of mid-ocean ridge basalts (MORB; Morgan, 1971, 1972), a proposition that has caused considerable debate (e.g. Campbell, 2005; Davies, 2005; Foulger, 2005; Foulger *et al.*, 2005; Campbell & Davies, 2006).

This early plume concept explicitly required that basalts from intra-plate ocean islands (OIB) result from mantle plumes originating from hotter, geochemically enriched (e.g. in potassium and light rare earth elements) materials in the deep lower mantle (Morgan, 1972), whereas MORB sample the ‘cooler’ and previously reworked/depleted asthenosphere (Morgan, 1972; Zindler & Hart, 1986; Hofmann, 1997) that must be shallow because sub-ridge mantle upwelling is a passive response to plate separation (Morgan, 1972; McKenzie & Bickle, 1988). The mantle plume concept was widely adopted because of its convenience in explaining the enriched characteristics of OIB chemistry, and because mantle plume phenomena have been successfully produced through laboratory (e.g. Campbell & Griffiths, 1990) and computer (e.g. Davies, 1999, 2005) simulations. However, the lack of geophysical means to detect mantle plumes unambiguously (e.g. Julian, 2005) makes the mantle plume concept remain a hypothesis to be tested and debated (e.g. Campbell, 2005; Davies, 2005; Foulger, 2005; Foulger *et al.*, 2005; Niu, 2005; Campbell & Davies, 2006). Consequently, petrological and geochemical data have been predominantly used as the primary basis on which to discuss the petrogenesis of OIB and to infer the origin and possible properties of ‘mantle plumes’ (e.g. Hofmann, 1997; Herzberg & O’Hara, 2002; Green & Falloon, 2005; Sobolev *et al.*, 2005; Herzberg *et al.*, 2007).

The geochemistry and petrology of OIB can be used to infer mantle potential temperatures (T_P ; e.g. Herzberg & O’Hara, 2002; Herzberg & Asimow, 2008), which must be high if the OIB sources form part of deep-rooted thermal mantle plumes, but should be low if the OIB sources are enriched materials with reduced solidus temperatures in the shallow mantle (Niu, 2005). Although this concept is straightforward, the calculated T_P values reported in the literature are highly model dependent (e.g. Green *et al.*, 2001; Green & Falloon, 2005; Putirka, 2005, 2008*a*, 2008*b*;

Herzberg *et al.*, 2007; Lee *et al.*, 2009). Because mantle source materials are probably heterogeneous on all scales and geochemically enriched OIB-like basalts are widespread (although volumetrically small) along ocean ridges and at near-ridge seamounts (e.g. Batiza & Vanko, 1984; Zindler *et al.*, 1984; Langmuir *et al.*, 1986; Castillo & Batiza, 1989; Sinton *et al.*, 1991; Mahoney *et al.*, 1994; Niu *et al.*, 1996, 1999, 2001, 2002; Niu & Batiza, 1997; Castillo *et al.*, 1998, 2000, 2010), OIB geochemistry alone cannot convincingly resolve whether their source materials originate from deep ‘mantle plumes’ or from concentrated (versus diluted beneath ocean ridges) heterogeneities in the upper mantle.

In this contribution, we do not attempt to resolve the ‘mantle plume’ debate, nor to model the petrogenesis of any particular OIB suite, but instead we discuss some geodynamic implications of a recent finding by Humphreys & Niu (2009) that oceanic lithosphere thickness variation exerts the first-order control on the geochemistry of OIB on a global scale, despite the importance of other effects such as mantle compositional heterogeneity and mantle T_P variations. The conclusions of Humphreys & Niu (2009) confirm earlier studies (e.g. Ellam, 1992; Haase, 1996) based on much more limited datasets.

THE PHILOSOPHY

The chemical characteristics of basalts are a complex function of fertile mantle composition, the P – T conditions of mantle melting and shallow-level melt differentiation processes. An important task for the petrologist is to distinguish the effects of these variables on melt composition. Shallow-level differentiation processes may be very complex (e.g. O’Hara, 1977), but can be corrected for, to a first approximation, by projecting to an Mg-number [$\text{Mg}/(\text{Mg} + \text{Fe})$] value of ≥ 0.72 , considered appropriate for melts in equilibrium with the mantle (e.g. Niu *et al.*, 1999; Niu & O’Hara, 2008). The composition of these near-primary mantle melts must then reflect either varying melting conditions or mantle compositional variations or both. This approach has been successful in elucidating the dynamics of mantle melting beneath ocean ridges, linking MORB chemistry with physical parameters such as ocean ridge axial depth (Dick *et al.*, 1984; Klein & Langmuir, 1987; Niu & O’Hara, 2008) and plate spreading rate (Niu & Hekinian, 1997*a*) on a global scale. Such success is expected because, despite small-scale complexities, mantle melting is a physical process, which must leave its chemical imprint on the resultant melt.

For intra-plate OIB magmatism, the only known or best constrained physical variable is the thickness of the oceanic lithosphere (L) on which the volcanic islands are built (Haase, 1996; Humphreys & Niu, 2009). It has long been accepted that oceanic lithosphere increases in thickness as a result of thermal contraction as it ages away from the

ridge at which it was first generated (e.g. Parsons & Sclater, 1977; Phipps Morgan & Smith, 1992; Stein & Stein, 1992); this is one of the basic tenets of plate tectonics. If we assume that intra-plate magma generation occurs in the sub-lithospheric mantle (likely to be the upper portion of the seismic low-velocity zone) by decompression melting, then OIB chemistry is expected to vary as a function of L ; that is, the lithosphere exerts a 'lid effect' (Niu & Hékinian, 1997*a*; Niu & O'Hara, 2007, 2008; Humphreys & Niu, 2009). Aspects of OIB chemistry that cannot be explained by the lid effect must be caused by other variables such as mantle potential temperature (T_P) or more probably mantle source compositional (X_{FM}) variation.

THE LID EFFECTS AND ITS GEODYNAMIC IMPLICATIONS

Humphreys & Niu (2009) used OIB samples with $\text{SiO}_2 < 53$ wt % from the global GEOROC database (<http://georoc.mpch-mainz.gwdg.de/georoc/>), corrected these data for fractionation effects to $\text{Mg-number} = 0.72$ (see Niu *et al.*, 1999; Niu & O'Hara, 2008), and excluded samples from volcanoes whose eruption ages are unknown and whose crustal ages at the time of volcanism cannot be reliably obtained for calculating the lithosphere thickness ($L = 11t^{1/2}$, where L is the oceanic lithosphere thickness in kilometres and t is the age in million years; Parsons & Sclater, 1977; Phipps Morgan & Smith, 1992; Stein & Stein, 1992). This data filtering resulted in 12 996 OIB samples from 115 islands in the Pacific (67 islands), Atlantic (38 islands) and Indian (10 islands) oceans. Humphreys & Niu (2009) evaluated the data using island-averages (i.e. 115 data points representing the 115 islands). Despite the fact that large compositional variations exist on any given island, they justified that such averaging is necessary and valid because the purpose is not to understand the petrogenesis of a particular basalt type, nor to evaluate X_{FM} variation, but to examine the bulk response of the entire volcanic systems to the potential control of L during island-building magmatism (i.e. over ~ 2 – 2.5 Myr) where L is essentially constant. In this case, within-island basalt compositional variation must be caused by factors or processes other than the effect of the L control and should be averaged out.

Here we average the data further within a number of 10 km lithosphere thickness intervals regardless of geographical location or ocean basin, the number of islands, the number of samples and range of basalt compositional variation within a given island (See Table 1 and Fig. 1; see also Electronic Appendix A, which is available for downloading at <http://www.petrology.oxfordjournals.org>). This heavy averaging is intended to objectively average out the effects of variables other than the L variation (see Niu & O'Hara, 2008; Humphreys & Niu, 2009).

The effect of oceanic lithosphere thickness (L)—the lid effect

The systematic variation of major elements Si_{72} , Ti_{72} , Al_{72} , Fe_{72} , Mg_{72} and P_{72} (the subscript 72 denotes the corresponding oxides corrected for fractionation effects to $\text{Mg-number} = 0.72$) and primitive-mantle normalized rare earth element (REE) ratios $[\text{La}/\text{Sm}]_N$ and $[\text{Sm}/\text{Yb}]_N$ as a function of L (Fig. 1) is best interpreted as resulting from the lid effect (see below). The lid effect shown by the 11 interval averages is more pronounced than that defined by the 115 island-averaged data (Humphreys & Niu, 2009) because, as intended, the heavy averaging smoothes out the effects of other factors such as mantle source heterogeneity that are known to vary in OIB from different islands, geographical locations and ocean basins.

Peridotite melting experiments (e.g. Jaques & Green, 1980; Stolper, 1980; Walter, 1998) and modelling efforts (Niu & Batiza, 1991; Niu, 1997; Walter, 1998) show that SiO_2 , Al_2O_3 , FeO , MgO and CaO contents in mantle melts depend on the melting pressure. SiO_2 (strongly), Al_2O_3 (moderately) and CaO (weakly) decrease, whereas MgO (strongly) and FeO (strongly to moderately) increase with increasing pressure of melting. Therefore, the decrease of mean Si_{72} , Al_{72} and Ca_{72} (weak) and increase of mean Mg_{72} and Fe_{72} in OIB with increasing L at the time of OIB volcanism is consistent with increasing pressures of mantle melting from beneath thin lithosphere to beneath thickened lithosphere. On the other hand, predictably the abundances of incompatible element oxides such as TiO_2 and P_2O_5 in mantle melts must increase with decreasing extents of melting. Therefore, the increase of mean Ti_{72} and P_{72} in OIB with increasing L at the time of OIB volcanism is consistent with decreasing extents of melting (F) as L increases (see Electronic Appendix A for more detailed discussion). Because La is more incompatible than Sm and Sm is more incompatible than Yb during mantle melting, the systematic $[\text{La}/\text{Sm}]_N$ and $[\text{Sm}/\text{Yb}]_N$ variation is also consistent with the lid effect (see below).

Figure 2, modified from Humphreys & Niu (2009), explains the lid effect in P – T space. For convenience, let us first assume that melting takes place in the sub-lithospheric mantle as a result of decompression of the asthenosphere that upwells adiabatically. The asthenospheric mantle begins to melt when it intersects the solidus. Continued upwelling is accompanied by continued decompression melting. As a result, the amount of melt produced or the extent of melting (F) from a given parcel of mantle (M_I) is proportional to the amount of vertical decompression (i.e. $P_o - P_I$). The lithosphere thus limits the vertical extent of decompression. Melting beneath thick lithosphere stops at a greater depth, and produces less melt (high Ti_{72} and P_{72}) with a high-pressure (P) signature (high Fe_{72} , Mg_{72}

Table 1: Averages of global OIB data with respect to ~10 km lithosphere thickness (L) intervals

	[1]	[2]	[3]	[4]	[5]	[6]	[7]	[8]	[9]	[10]	[11]	R
L interval (km):	0	<10	10–20	20–30	30–40	40–50	50–60	60–70	70–80	80–90	>90	
L interval mean (km):	0.00	8.93	16.29	25.53	35.75	47.78	54.77	64.07	77.70	83.56	90.00	
L interval (σ):	–	0.899	2.132	3.256	3.437	1.273	1.865	3.618	1.572	0.560	–	
<i>N</i> [1]	2054	42	383	533	30	442	192	175	620	152	8373	
Si ₇₂	47.400	46.658	47.547	47.239	46.584	45.439	45.809	44.132	45.267	45.864	44.617	–0.825
Si ₇₂ σ	2.511	1.486	1.434	1.450	1.255	1.938	2.839	2.361	2.294	2.918	2.733	(>99%)
Ti ₇₂	1.302	1.524	1.579	1.823	2.161	2.130	1.995	2.250	2.250	2.129	2.365	0.901
Ti ₇₂ σ	0.442	0.608	0.416	0.501	0.438	0.603	0.575	0.695	0.556	0.748	0.613	(>99.5%)
Al ₇₂	17.846	17.703	17.642	16.841	17.431	16.577	16.825	15.325	14.975	16.401	15.012	–0.879
Al ₇₂ σ	2.415	3.840	1.584	0.501	2.250	2.395	2.504	3.488	2.841	2.694	2.455	(>99.5%)
Fe ₇₂	7.998	7.703	7.799	8.288	7.832	8.202	7.937	9.323	9.115	7.680	9.482	0.600
Fe ₇₂ σ	1.590	2.864	1.009	1.289	1.627	1.982	2.288	2.662	2.321	2.511	1.897	(>95%)
Mn ₇₂	0.136	0.109	0.116	0.142	0.129	0.122	0.109	0.145	0.130	0.129	0.140	0.301
Mn ₇₂ σ	0.110	0.046	0.035	0.037	0.016	0.034	0.035	0.040	0.047	0.034	0.069	(>70%)
Mg ₇₂	11.050	11.493	11.230	11.626	11.396	11.591	11.523	12.733	12.557	11.590	12.632	0.751
Mg ₇₂ σ	1.229	1.797	0.706	0.883	0.915	1.303	1.468	2.105	1.820	1.724	1.525	(>99%)
Ca ₇₂	11.600	10.864	10.525	10.381	9.864	10.233	10.400	10.908	9.763	10.197	10.629	0.493
Ca ₇₂ σ	1.373	0.875	0.917	1.122	0.922	2.088	2.254	1.812	1.642	2.137	1.742	(>85%)
Na ₇₂	2.413	2.431	2.506	2.791	2.957	2.582	2.893	2.662	2.575	3.084	2.680	0.510
Na ₇₂ σ	0.417	0.590	0.347	0.389	0.423	0.705	0.589	0.757	0.502	0.538	0.626	(>85%)
K ₇₂	0.341	0.996	0.540	0.864	1.328	1.560	1.432	1.160	1.379	1.311	1.085	0.665
K ₇₂ σ	0.141	0.343	0.269	0.283	0.264	0.768	0.441	0.548	0.501	0.436	0.478	(>95%)
P ₇₂	0.190	0.494	0.300	0.385	0.541	0.590	0.515	0.511	0.489	0.651	0.568	0.745
P ₇₂ σ	0.081	0.141	0.174	0.131	0.168	0.280	0.173	0.197	0.158	0.216	0.234	(>99%)
<i>N</i> [2]	889	39	246	305	35	205	124	107	310	90	2360	
[La/Sm] _N	1.216	2.710	2.186	2.302	3.213	3.228	3.648	4.171	2.947	2.983	3.327	0.682
[La/Sm] _N σ	0.231	0.243	0.856	0.507	0.544	0.840	1.260	1.672	0.917	0.877	1.346	(>98%)
<i>N</i> [3]	860	38	239	298	35	208	120	104	266	90	2349	
[Sm/Yb] _N	1.733	3.606	2.617	2.682	3.935	4.539	4.647	4.281	4.908	4.095	4.698	0.819
[Sm/Yb] _N σ	0.307	0.700	0.527	0.469	0.520	0.798	0.847	0.830	0.914	0.624	1.319	(>99%)
<i>N</i> [4]	343	37	208	179	16	185	91	136	224	22	1200	
¹⁴³ Nd/ ¹⁴⁴ Nd	0.513036	0.512762	0.512931	0.512947	0.512902	0.512877	0.512786	0.512832	0.512775	0.512903	0.512901	–0.355
¹⁴³ Nd/ ¹⁴⁴ Nd σ	0.000110	0.000077	0.000036	0.000033	0.000034	0.000044	0.000034	0.000031	0.000076	0.000034	0.000062	(>75%)
<i>N</i> [5]	520	43	227	237	37	257	111	214	287	38	1623	
⁸⁷ Sr/ ⁸⁶ Sr	0.703011	0.704262	0.703540	0.703561	0.703688	0.703503	0.703980	0.703493	0.704550	0.703724	0.703717	0.355
⁸⁷ Sr/ ⁸⁶ Sr σ	0.000108	0.000363	0.000535	0.000476	0.000352	0.000509	0.000496	0.000330	0.000537	0.000270	0.000438	(>75%)
<i>N</i> [6]	299	30	171	187	20	213	92	138	153	40	1345	
²⁰⁶ Pb/ ²⁰⁴ Pb	18.922	18.696	18.855	19.070	19.639	19.662	19.143	19.991	19.145	19.559	19.129	0.508
²⁰⁶ Pb/ ²⁰⁴ Pb σ	0.306	0.113	0.118	0.161	0.292	0.200	0.282	0.147	0.119	0.166	0.153	(>90%)
<i>N</i> [7]	299	30	170	187	20	213	92	138	150	40	1337	
²⁰⁷ Pb/ ²⁰⁴ Pb	15.558	15.565	15.569	15.578	15.601	15.614	15.584	15.680	15.593	15.599	15.565	0.389
²⁰⁷ Pb/ ²⁰⁴ Pb σ	0.031	0.021	0.023	0.019	0.041	0.033	0.045	0.024	0.026	0.016	0.022	(>75%)
<i>N</i> [8]	299	30	170	187	20	212	92	137	150	40	1247	
²⁰⁸ Pb/ ²⁰⁴ Pb	38.671	38.907	38.747	38.784	39.137	39.385	39.082	39.578	39.001	39.198	38.911	0.518
²⁰⁸ Pb/ ²⁰⁴ Pb σ	0.438	0.129	0.171	0.169	0.316	0.181	0.227	0.123	0.176	0.199	0.155	(>90%)
<i>N</i> [9]	40	8	83	61	–	26	36	12	–	–	363	
¹⁷⁶ Hf/ ¹⁷⁷ Hf	0.283123	0.282995	0.283048	0.283086	–	0.282875	0.282922	0.282914	–	–	0.283037	–0.493
¹⁷⁶ Hf/ ¹⁷⁷ Hf σ	0.000026	0.000110	0.000043	0.000015	–	0.000023	0.000030	0.000044	–	–	0.000048	(>70%)

L, lithosphere thickness (km) at the time of active volcanism for single ocean islands (see below and Humphreys & Niu, 2009 for details). Numbers [1]–[11] refer to 10 km lithosphere thickness intervals from 0 km (for [1]) to >90 km (>70 Myr old, for [11]). Column *R* gives correlation coefficients of within-interval mean lithosphere thickness with corresponding geochemical parameters and the levels of their statistical significance (e.g. >99%) (see Fig. 1). *N*[1]–*N*[9], number of samples averaged for major elements (*N*[1]) and other parameters immediately below the corresponding rows. All geochemical parameters (e.g. Si₇₂, [La/Sm]_N, ⁸⁷Sr/⁸⁶Sr) are averages (means) of *N* samples within the given 10 km lithosphere intervals, and σ refers to one standard deviation from the mean. All major element data used are basalts with SiO₂ < 53 wt % and also corrected for fractionation effect to Mg-number [Mg/(Mg + Fe)] = 0.72 (i.e. the significance of the subscript 72) to reflect mantle (vs crustal) signatures (see Niu & O'Hara, 2008; Humphreys & Niu, 2009). [La/Sm]_N and [Sm/Yb]_N are primitive mantle (Sun & McDonough, 1989) normalized REE ratios without correcting the fractionation effect that is negligible. All geochemical data are from the GEOROC database (<http://georoc.mpch-mainz.gwdg.de/georoc/>) with details described by Humphreys & Niu (2009). Lithosphere thickness intervals include the following islands (see Humphreys & Niu, 2009): [1] Darwin, Genovesa, Marchena and Pinta in the Pacific, and Iceland, Kolbeinsey and Vestmannaeyjar islands in the Atlantic; [2] Kerguelen and Foch in the Indian Ocean, Matotiri and Wolf in the Pacific; [3] Ile de l'Ouest and Amsterdam in the Indian Ocean, and Baltra, Easter Island, Rabida and Santa Cruz in the Pacific; [3] Heard in the Indian Ocean, Ascension and Faial in the Atlantic, and Espanola, Fernandia, Floreana, Isabela, Roca Redonda, Pinzon, San Cristobal and Santa Fe in the Pacific; [5] Flores, Graciosa, Pico and San Jerge in the Atlantic; [6] Terceira, Jan Mayen and São Miguel in the Atlantic, and Fangatufa, Gambier Islands, Mururoa atoll, Pitcairn, Rimatara, Rututu and Tubuai in the Pacific; [7] Inaccessible and Tristan da Cunha in the Atlantic, and Macquarie, Rapa and Raivavae in the Pacific; [8] St Helena in the Atlantic, and Mangaia, Mas a Tierra and Rarotonga in the Pacific; [9] Gough in the Atlantic, Aitutaki, Atiu, Bora Bora, Fatu Hiva, Fatu Huku, Hiva Oa, Huahine, Mas Afuera, Mehetia, Motane, Motu Nao, Nuku Hiva, Raiatea, Tahaa, Tahiti, Tahuata, Ua Huka and Ua Pou in the Pacific, and Mauritius in the Indian Ocean; [10] Eiao, Hatutu and Ross Island in the Pacific; [11] Bioko, Boa Vista, Chao, Deserta Grande, Fernando Poo, Fogo, Fuerteventura, Gran Canaria, Hierro, La Gomera, La Palma, Lanzarote, Maderia, Maio, Pagalu, Porto Santo, Principe, Sal, Santiago, São Tome, Tenerife, Trindade in the Atlantic, Ile aux Cochon, Ile de la Possession, Ile de l'Est and Reunion in the Indian Ocean, and Gardner Pinnacle, Hawaii, Kahoolawe, Kauai, La Perouse Pinnacle, Lanai, Maui, Molokai, Nihoa, Niihau, Oahu, Savaii, Tutuila and Upolu in the Pacific.

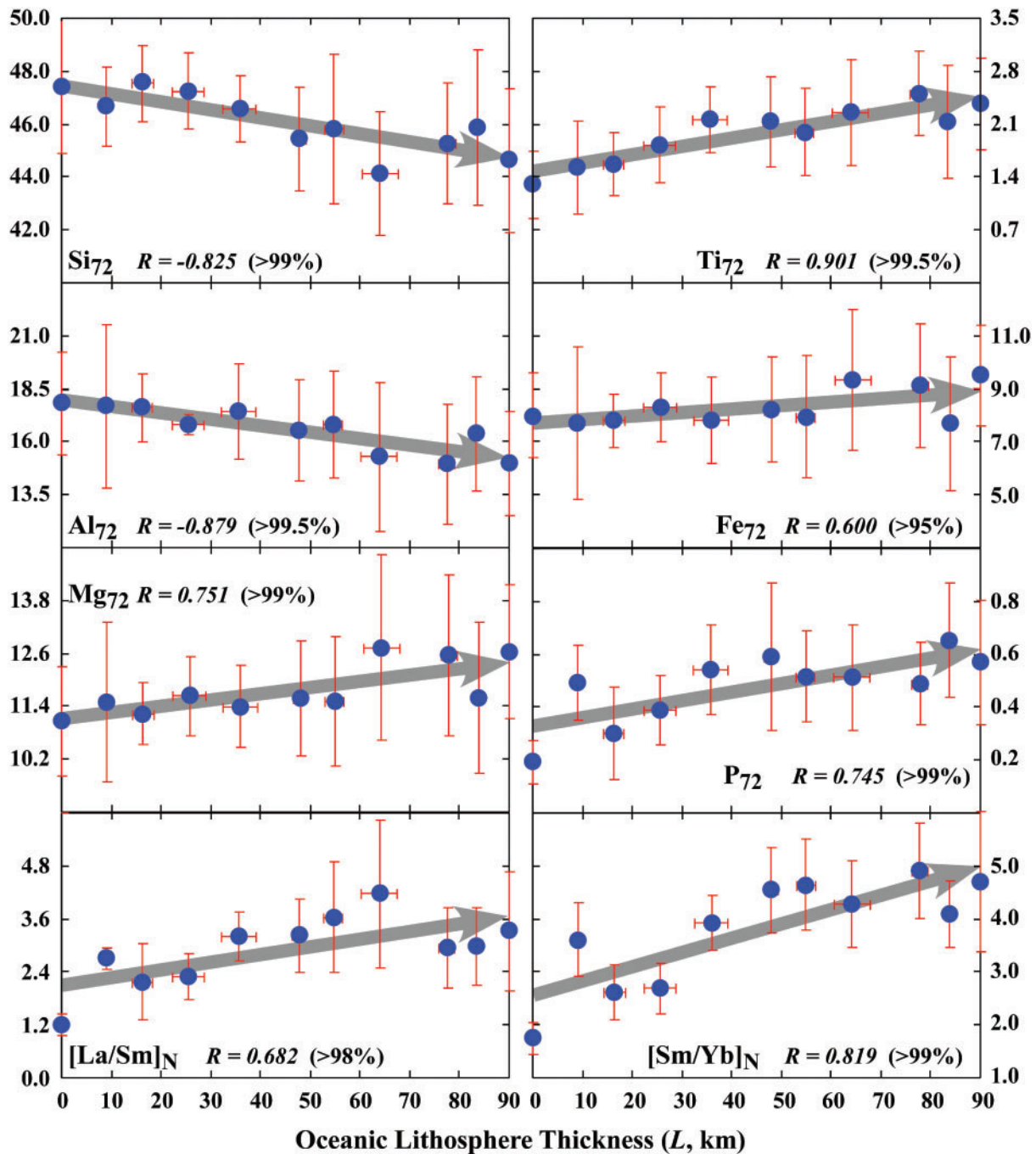


Fig. 1. Geochemical parameters normalized to Mg-number of 72 (e.g. Ti_{72} stands for weight per cent of TiO_2 corrected for fractionation effect to Mg-number = 0.72; see Niu *et al.*, 1999; Niu & O'Hara, 2008; Humphreys & Niu, 2009) before heavy averaging within each of the 10 km lithosphere thickness intervals regardless of geographical locations or ocean basins, the number of islands, the number of samples and lava compositional variation from a given island. The discussion in the text is based on these trends defined by the 11 averages. [See Table 1 for plotting data, Appendix Figs A1 and A2 for additional plots with discussion, and Humphreys & Niu (2009) for data details.]

and low Si_{72} and Al_{72}), whereas melting beneath thin lithosphere stops at a shallower depth, and produces more melt (low Ti_{72} and P_{72}) with a low- P signature (low Fe_{72} , Mg_{72} and high Si_{72} and Al_{72}). In other words, the lithosphere

thickness determines the mean F and P of melting beneath ocean basins.

It is conceptually important to note that the extent of melting (F) is the mass fraction of fertile mantle (FM)

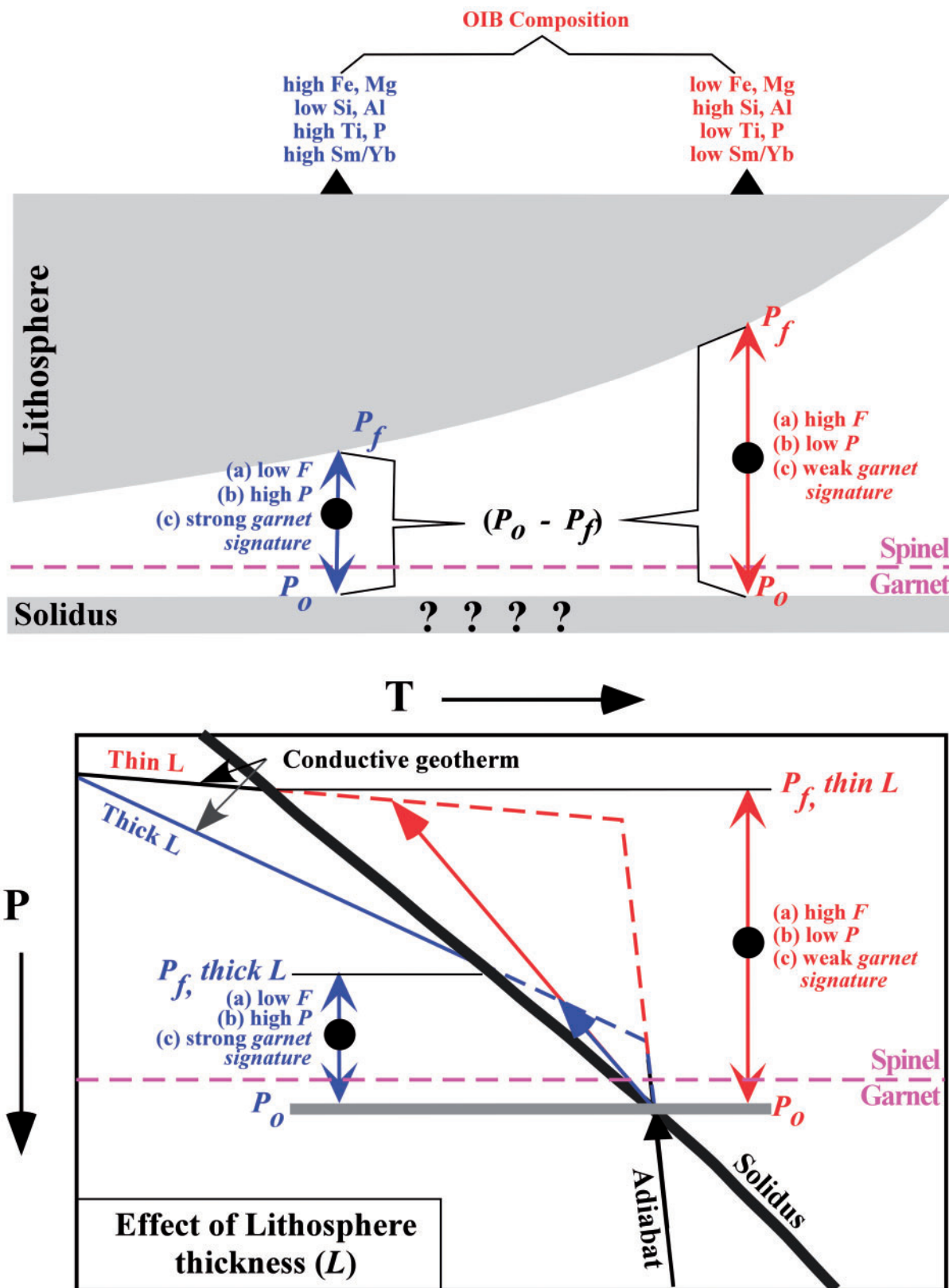


Fig. 2. Schematic illustration showing the lid effect to explain OIB compositional variation as a function of the lithosphere thickness (Fig. 1). Top, the base of the lithosphere limits the final depth of melting (P_f) leading to subdued extent of melting by reducing the vertical range of decompression ($P_o - P_f$), which is proportional to the extent of melting. The solid circles indicate conceptually the mean pressure of melting reflected in the geochemistry of the erupted OIB melts, hence the inverse correlation between the extent and pressure of melting (The pressure signature recorded in the OIB is actually the base of the lithosphere, P_f , as indicated in Fig. 4). Bottom, this concept is illustrated in pressure–temperature space. The adiabatically upwelling parcel of mantle begins to melt when intersecting the solidus at depth of P_o . Continued upwelling leads to continued decompression melting until the upwelling is blocked at P_f , the base of the lithospheric lid. The significance of all other elements is self-explanatory. It should be noted that the solidus depth in the upper panel is assumed to be constant to illustrate the concept. Modified from Niu & Hékinian (1997a), Niu *et al.* (2001), Niu & O’Hara (2008) and Humphreys & Niu (2009).

melted and is not the same as the mass of melt produced (M_M); that is, $M_M = F \times M_{FM}$. Therefore, no correlation is expected between the size of intra-plate oceanic islands and L . This means that M_{FM} , or fertile mantle material flux, is an important factor when comparing melt volumes (M_M) between intra-plate ocean islands. This concept is relevant to the ‘mantle plume’ debate.

The implications of the above discussion and our observations in Fig. 1 are profound and allow us to make several important statements.

Oceanic lithosphere thickness exerts the first-order control on global OIB geochemistry

In the upper panel of Fig. 2, we show the location of the mantle solidus with question marks because this is a material property and its actual depth is unlikely to be constant, but can vary significantly because of mantle compositional variations (X_{FM}), in particular the likely varying abundances of volatiles (e.g. H_2O and CO_2) and alkalis, whose enrichments will deepen the solidus and cause the onset of melting at greater depths (Wyllie, 1988a). In the lower panel of Fig. 2, we show only one subsolidus adiabatic path because we assume for conceptual clarity that T_P is the same beneath all oceanic lithosphere (or beneath all intra-plate ocean islands). This is unlikely to be true, although to determine T_P precisely from OIB chemistry or petrology is not straightforward and is model dependent (see above and below). A hotter parcel of rising mantle will intersect the solidus deeper and potentially melt more than a cooler parcel of rising mantle. Consequently, variations in the initial depth of melting as a result of X_{FM} and T_P variation will also influence OIB compositions. However, these two variables must have secondary effects because they do not overshadow the effect of L variation that is prominent on a global scale as illustrated in Fig. 1. In other words, the correlations in Fig. 1 would not exist if the lid effect is less important than source and temperature effects. This is actually not surprising because the L variation is of the order of tens of kilometres (up to 90 km; see Fig. 1). The T_P variation required to compensate the lid effect in terms of ‘decompression melting’ would probably be unrealistically large (>300 K?). Furthermore, even if such large T_P variation were possible, it is not obvious why T_P variations beneath ocean islands would spatially correlate with lithosphere thickness (or age). Therefore, we conclude that oceanic lithosphere thickness (L) exerts the first-order control on the geochemistry of global OIB by physically limiting the mean F and depth (i.e. pressure, P) of melting beneath the oceanic lithosphere. It is worth noting that if OIB are indeed of hot mantle plume origin, ‘thermal erosion’ could then thin the lithosphere beneath ocean islands on local scales, but Fig. 1 suggests that this effect, if present at all, is not significant.

We suggest that the concept of the lid effect also applies to the petrogenesis of basalts erupted in continental settings, but do not consider this further here.

The ‘garnet signature’ in OIB is diluted by shallow melting confined by the lithosphere

The increase in OIB Ti_{72} , P_{72} , $[La/Sm]_N$ and $[Sm/Yb]_N$ (Fig. 1) with increasing L is best explained by decreasing F as the result of a progressively restricted vertical interval of decompression (i.e. $P_o - P_f$). The decrease of these geochemical parameters with decreasing L can conversely be considered as a result of dilution; that is, the abundances of the incompatible elements P, Ti, La (vs Sm) and Sm (vs Yb) are the highest in low- F melts at an early stage of decompression melting, and become progressively diluted in the melts during the continued decompression melting that is possible with decreasing L . The $[Sm/Yb]_N$ variation is particularly informative (Fig. 1) because the greater than unity variation of this ratio indicates the presence of the familiar ‘garnet signature’ in OIB melts (Salters & Hart, 1989; Hirschmann & Stolper, 1996; Niu *et al.*, 1999; Putirka, 1999). Mantle melting beneath all intra-plate ocean islands probably begins in the garnet peridotite facies, thus imprinting the garnet signature on melt compositions (i.e. $[Sm/Yb]_N > 1$). Importantly, the intensity of the garnet signature decreases with decreasing L (Fig. 1) from ~ 5 in average OIB melts erupted on the thickest lithosphere to ~ 1.7 in average OIB melts erupted on the thinnest lithosphere. This is the simplest manifestation of the dilution effect. Although mantle melting beneath all intra-plate ocean islands probably begins in the garnet peridotite facies, decompression melting continues in the spinel peridotite facies below thin lithosphere, thus diluting the garnet signature in the melt. The extent of dilution is limited by the amount of melting in the spinel peridotite facies, which is ultimately constrained by L ; hence the positive correlation between $[Sm/Yb]_N$ and L (Fig. 1).

Sr–Nd–Pb–Hf isotopes in OIB show both lid and source effects

It is important to note that although varying F because of the varying L can explain the varying abundances and ratios of incompatible elements in Fig. 1, quantitatively this is inadequate without invoking the presence of a highly enriched component (or components) in the OIB source regions. Such an enriched component has a lower solidus temperature than the ambient mantle and melts first. Hence, the product of early stage melting (i.e. near-‘solidus’ melting) is dominated by this enriched component and has elevated abundances of incompatible elements. The enriched component in the melt is diluted progressively with continued decompression melting of the more depleted, or, rather, less enriched, source component(s). The ‘dilution’ effect, reflected in geochemical variation

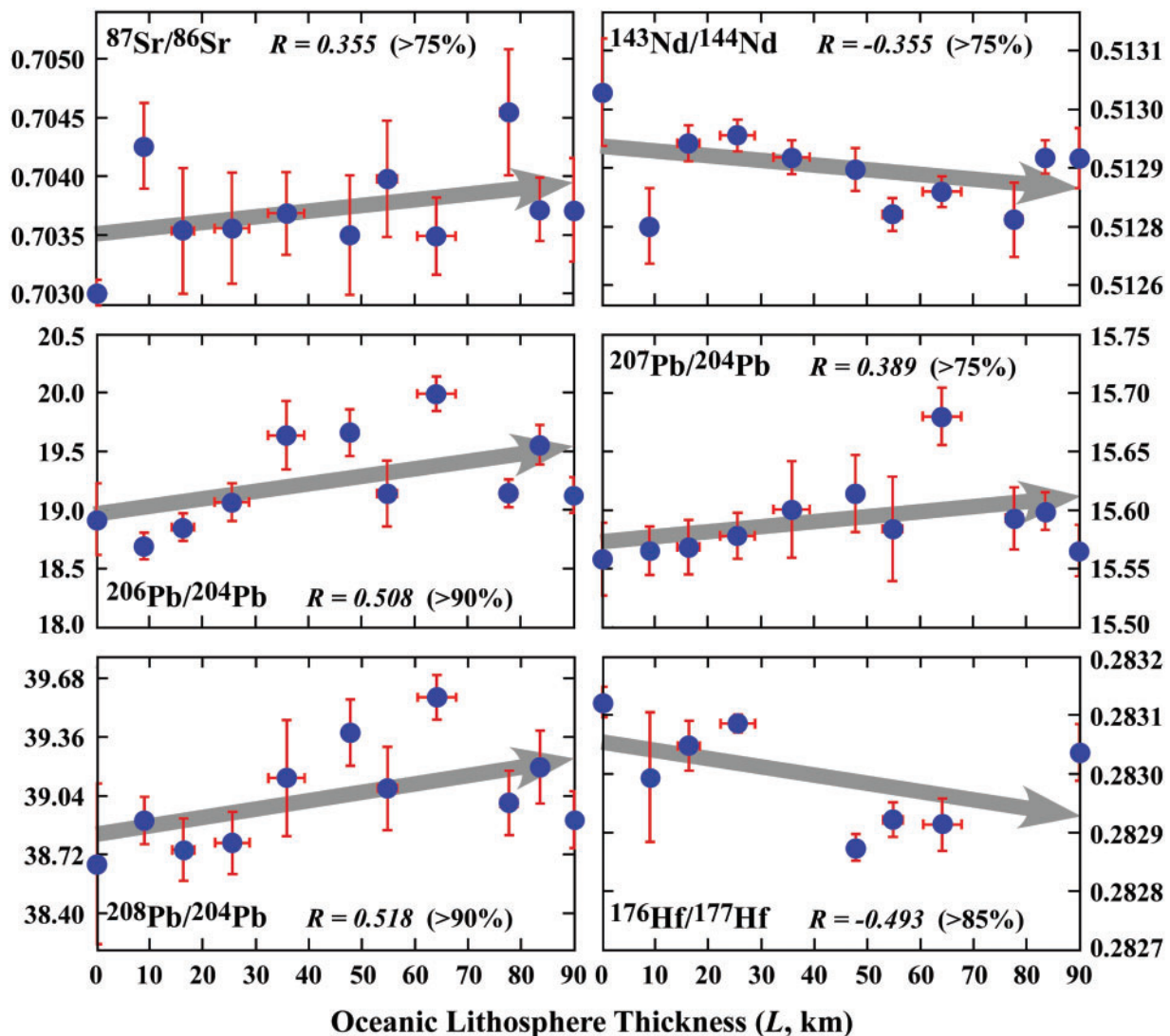


Fig. 3. Average radiogenic isotope compositions of global OIB data plotted as a function of lithosphere thickness. The averaging is the same as in Fig. 1. [See Table 1 for plotting data, Appendix Figs A3 and A4 for further discussion, and Humphreys & Niu (2009) for data details.]

diagrams, is equivalent to mixing of melts from a compositionally heterogeneous mantle source containing an enriched or easily melted component dispersed in a more depleted peridotitic matrix (Niu *et al.*, 1996, 2002; Niu & Batiza, 1997).

If the major OIB source materials are of ancient history, then radiogenic isotope variations should be coupled with incompatible element variations. That is, an enriched source with higher $^{87}\text{Sr}/^{86}\text{Sr}$, $^{206}\text{Pb}/^{204}\text{Pb}$ and lower $^{143}\text{Nd}/^{144}\text{Nd}$, $^{176}\text{Hf}/^{177}\text{Hf}$ must have higher ratios of more to less incompatible elements (i.e. high La/Sm, Rb/Sr, U/Pb, Nd/Sm and Hf/Lu) than a less enriched or depleted source. This would suggest that OIB erupted on thickened lithosphere resulting from lower extents of melting should

have a stronger signature of the more enriched component (less diluted) with higher $^{87}\text{Sr}/^{86}\text{Sr}$, $^{206}\text{Pb}/^{204}\text{Pb}$ and lower $^{143}\text{Nd}/^{144}\text{Nd}$, $^{176}\text{Hf}/^{177}\text{Hf}$ than OIB erupted on thin lithosphere. This is indeed broadly the case as shown in Fig. 3, consistent with the lid effect. However, the correlations of these isotopic ratios (versus major and trace elements in Fig. 1) are poor; this may have several causes: (1) isotopes more faithfully reflect source heterogeneity because the latter is independent of melting conditions (only the dilution effect); (2) fewer data are available at a given lithosphere thickness interval for averaging; (3) recent source enrichments that may have led to element–isotope decoupling (Mahoney *et al.*, 1994; Niu *et al.*, 1996; Niu & O'Hara, 2003, 2009). Over 20 years ago, Park (1990) in an

unpublished PhD thesis recognized broad correlations of OIB Sr and Nd isotope composition with seafloor age at the time of eruption, but did not develop this idea further.

OIB compositions record final depth of melting (P_f), not initial depth of melting (P_o)

Over the past two decades, the petrological community has attempted to extract mantle solidus P - T information (i.e. P_o and T_o) from the chemistry of basalts (e.g. Klein & Langmuir, 1987; Niu & Batiza, 1991; Kinzler & Grove, 1992; Langmuir *et al.*, 1992; Niu, 1997; Green *et al.*, 2001; Herzberg & O'Hara, 2002; Green & Falloon, 2005; Putirka, 2005, 2008a, 2008b; Herzberg *et al.*, 2007; Herzberg & Gazel, 2009; Lee *et al.*, 2009) by comparing basalt chemistry with experimental data on mantle peridotite melting (e.g. Jaques & Green, 1980; Stolper, 1980; Falloon & Green, 1987, 1988; Kinzler & Grove, 1992; Hirose & Kushiro, 1993; Baker & Stolper, 1994; Herzberg & Zhang, 1996; Walter, 1998; Hirschmann, 2000). Figure 1 shows convincingly that although OIB geochemistry does preserve a pressure (P) signature, the correlations of OIB chemistry with L suggest that these P signatures represent the final depth of melting (P_f) or melt equilibration rather than initial depth of melting (P_o) or the mantle solidus.

For convenience, we can combine the various P -indicating petrological parameters from Fig. 1 into a single P -parameter, expressed in terms of lithosphere thickness using a polynomial regression (with $R^2 = 0.942$) (Fig. 4). The fact that OIB chemistry correlates significantly with L (or age of the oceanic lithosphere) suggests the likelihood that the best a well-calibrated basalt-based thermobarometry method can do is to obtain the P - T conditions of the final depth of melting or melt equilibration (i.e. P_f and T_f), because OIB do not contain unambiguous signals of P - T conditions deeper and hotter than the base of the lithospheric lid (Figs 1 and 4). Therefore, caution is necessary when using basalt-based thermobarometers to infer the initial depth and temperature of melting unless the lid effect is properly corrected for. In this context it is important to recognize that melt–solid equilibration is extremely efficient under sub-lithospheric mantle conditions.

Because MgO in primary mantle melts is positively related to both P and T (SiO_2 is negatively related to P) and because the 'dry' mantle solidus has a positive slope in P - T space, an estimated high P leads to high T (or vice versa) for all basalt-based thermobarometers. For example, L is essentially zero beneath Iceland but ~ 90 km beneath Hawaii; thus primitive Icelandic basalts should have a lower MgO content and lower P signature than Hawaiian basalts. As a result the estimated T_P will be significantly higher for Hawaii than for Iceland. Indeed, Putirka (2005) estimated $T_P = 1583^\circ\text{C}$ for Iceland and

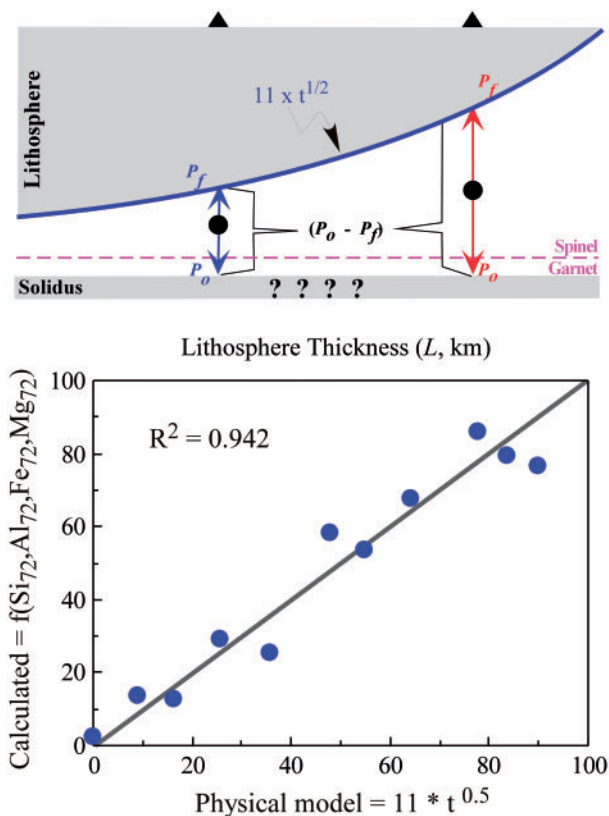


Fig. 4. Top, simplified from Fig. 2 to illustrate the concept of mean extent and pressure of melting recorded in OIB. Bottom, a multivariate regression analysis can express the lithosphere thickness in terms of several pressure-sensitive parameters in Fig. 1 (i.e. major element oxides Si_{72} , Al_{72} , Fe_{72} and Mg_{72}). This simple exercise is meant to emphasize that OIB record faithfully only the final depth of melting or melt equilibration (P_f , thick blue curve) but neither solidus (unconstrained) nor 'mean pressure of melting'.

1687°C for Hawaii. Similarly, Herzberg & Gazel (2009) calculated a maximum T_P of 1460°C for Iceland and 1590°C for Hawaii. However, the two sets of calculations are clearly very different, with $\Delta T_P > 120^\circ\text{C}$ for Iceland and $\sim 100^\circ\text{C}$ for Hawaii. This is a simple demonstration of the model dependence of such basalt-based thermobarometers. The two models do, however, have one thing in common—that $T_{P \text{ Hawaii}}$ is greater than $T_{P \text{ Iceland}}$ by $> 100^\circ\text{C}$. It is unknown to what extent this T_P difference is due to the lid effect (~ 90 km or 3 GPa). We suggest that the calculated T_P values should not be considered valid without correcting for the lid effect.

In the above context, it is worth emphasizing a basic petrological concept about MORB petrogenesis. With essentially zero L at mid-ocean ridges, it is unlikely that MORB preserve T_o or T_P as demonstrated by Niu & O'Hara (2008). It is thus not surprising that MORB are characterized by low- P chemical signatures on a global scale (e.g. O'Hara, 1968; Walker *et al.*, 1979).

The oceanic lithosphere as a ‘thermal boundary layer’ has petrological significance

There has been some disagreement about the definition of ‘lithosphere’ (e.g. Anderson, 1995, 2011). It may indeed be more appropriate to define the ‘lithosphere’ as a near-surface strong mechanical boundary layer (Anderson, 1995), in which case the thickness of the ‘mechanical boundary layer’ would correspond to a maximum thickness of ~60 km bounded by an isotherm of 600°C, which is below the mantle solidus and would therefore have no petrological significance. The depth and nature of the lithosphere–asthenosphere boundary (LAB) has also been a subject of recent debate. For example, Rychert & Shearer (2009), on the basis of a global receiver function study, observed a shear-wave velocity drop at an average depth of 70 ± 4 km beneath the ocean basins, which they attributed to the LAB. However, this is the average depth using observations from a number of ocean islands on ocean crust of varying age, and thus does not reflect the possible LAB variation as a function of lithosphere age. On the other hand, Kawakatsu *et al.* (2009) reported high-quality observations of both Ps and Sp conversions at LAB depths on the basis of the long-term operation of a number of low-noise borehole seismic observatories on ocean floor of varying age in the western Pacific. They showed nicely an age-dependent LAB depth variation that is consistent with an isotherm of ~1100°C using a thermal model with $T_P = 1315^\circ\text{C}$ (McKenzie *et al.*, 2005). An abrupt V_s drop below the LAB requires the present of melt in the uppermost asthenosphere (Kawakatsu *et al.*, 2009; Fischer *et al.*, 2010; Kumar & Kawakatsu, 2011), which is in fact required by petrological models for OIB petrogenesis (see fig. 10 and discussion of Niu & O’Hara, 2009; Niu, 2009).

Here, as in an earlier study (Humphreys & Niu, 2009), we follow the traditional approach of defining the oceanic lithosphere as a thermal boundary layer whose thickness is proportional to the square root of age (Parsons & Sclater, 1977; Phipps Morgan & Smith, 1992; Stein & Stein, 1992) and reaches its full thickness (~90 km) at an age of ~70 Ma. Various workers have attempted to constrain the temperature at the base of the lithosphere. Parsons & Sclater (1977) proposed that it approximates an ~1250°C isotherm, whereas Kawakatsu *et al.* (2009) arrived at ~1100°C with $T_P = 1315^\circ\text{C}$ (McKenzie *et al.*, 2005). The plate model (Stein & Stein, 1992) suggests an isotherm of 1450°C at the base of the lithosphere, which may be too hot (see McKenzie *et al.*, 2005).

The significant correlation of OIB chemistry with the thickness of the oceanic lithosphere (Figs 1 and 4) suggests that the base of the lithosphere (i.e. LAB) may be considered as a natural peridotite solidus below which upwelling mantle can melt, and above which the material is

under subsolidus conditions (Niu *et al.*, 2002; Niu & O’Hara, 2003, 2009). Conceptually, treating the base of the lithosphere as the solidus means that if the mantle is anhydrous it cannot be an isotherm because the ‘dry’ solidus has a non-zero positive slope in P – T space (see the lower panel of Fig. 2 and Fig. 5a). However, the LAB could be consistent with the pargasite dehydration solidus of H₂O–CO₂-bearing mantle peridotite (Fig. 5; see Green, 1971; Green & Liebermann, 1976; Wyllie, 1988a; Wyllie & Ryabchikov, 2000; Green & Falloon, 2005; Green *et al.*, 2010; Niu *et al.*, 2010), which is nearly an isotherm (~1100°C) at depths less than ~90 km (Fig. 5b). Figure 5b also shows that oceanic geotherms for plate ages of 20–80 Ma, interpolated from the work of Kumar & Kawakatsu (2011), are consistent with an adiabat with $T_P = 1315^\circ\text{C}$ (McKenzie *et al.*, 2005), and their intercepts with the pargasite dehydration solidus indicate the base of the lithosphere (or LAB) at the corresponding plate age. It should be noted that the pargasite dehydration solidus becomes isobaric at ~90 km (Fig. 5a), which can effectively explain why oceanic lithosphere older than 70 Ma cannot be thicker than ~90 km. We elaborate this concept in detail in a later section.

The geochemistry of OIB requires dynamic upwelling and decompression melting

We assumed above that mantle melting beneath intra-plate ocean islands occurs by decompression of rising fertile mantle without justification. We often do not justify assumptions of this sort because we take it for granted that they must be the case, in particular if we accept that OIB are of mantle plume origin without challenging the assumptions built into the mantle plume hypothesis. However, a brief analysis of our observations is useful for a clearer understanding of the dynamics of mantle melting beneath intra-plate ocean islands. Figures 1 and 4 indicate the relationship of the extent (F) and pressure (P) of melting with oceanic lithosphere thickness (L) inferred from OIB geochemistry: $F \propto 1/L$ [or $F \propto (P_o - P_f)$ (although P_o is uncertain)] and $P \propto L$. To explain the F – P – L relationship, we can consider two physical scenarios shown in Fig. 6, as follows.

- (1) The sub-lid mantle (i.e. $P_o - P_f$ in the seismic low-velocity zone) is close to the solidus, producing melt, which has a tendency to migrate upwards and concentrate just below the base of the lithosphere because of its buoyancy (small red arrows). Melt subsequently extracted/erupted vertically records the lid effect and explains the F – P – L relationship.
- (2) Columnar upwelling (large red arrows) of fertile mantle material from depths below the solidus and its consequent decompression melting produces melt, which, when extracted or erupted, explains the F – P – L relationship.

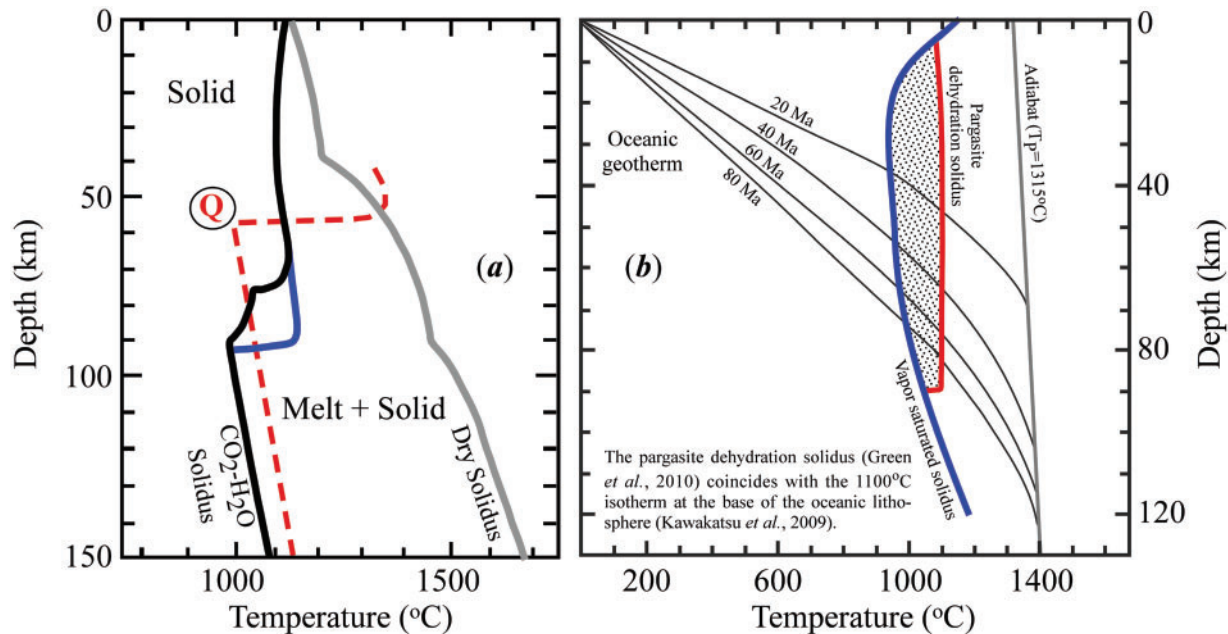


Fig. 5. (a) Selected phase boundaries for peridotite-H₂O-CO₂. The dry solidus is from Takahashi & Kushiro (1983); the 'wet solidus' is from Wyllie (1987, 1988a, 1988b), Green (1991) and Green & Falloon (1998, 2005). The short blue curve is our suggested position for the high-pressure part of the dehydration solidus for H₂O-CO₂-bearing amphibole-peridotite modified from Green (1973) and Green & Falloon (1998, 2005). The red dashed line is part of the peridotite-CO₂ solidus (Presnall & Gudfinnsson, 2008), where the 'kink' is equivalent to point 'Q' for model CaO-MgO-SiO₂-CO₂ system of Wyllie and coworkers (Lee & Wyllie, 2000; Lee *et al.*, 2000). We emphasize the importance of H₂O + CO₂, not CO₂ alone, in the seismic low-velocity zone (LVZ). We suggest (1) that the near-isothermal portion (near vertical, $dT/dP \approx 0$, $< \sim 90$ km) of the wet solidus corresponds to the base of the lithosphere $< \sim 80$ Myr old, and (2) that the isobaric portion (short blue horizontal line, $dP/dT \approx 0$, ~ 90 km) of the wet solidus determines the depth of the LAB [i.e. ~ 90 km beneath the mature ($> \sim 70$ Myr) oceanic lithosphere]. (b) Schematic illustration of the vapor (H₂O)-saturated and pargasite dehydration solidi after Green *et al.* (2010). Also shown are oceanic geotherms for plate ages of 20, 40, 60 and 80 Ma (interpolated from Kumar & Kawakatsu, 2011). The geotherms are consistent with an adiabat with $T_p = 1315^\circ\text{C}$ in the deeper mantle (McKenzie *et al.*, 2005), and their intercepts with the pargasite dehydration solidus indicate the base of the lithosphere (or LAB) at the corresponding ages.

Scenario (1) requires (a) that the melt pockets have no lateral communication, otherwise melt mixing would readily destroy the F - P - L relationship, and (b) that statistically the melt could erupt anywhere or everywhere in the plate interior if zones of weakness (cracks or faults) exist in the lithosphere that permit magma migration. This can indeed explain the formation of seamounts of alkali basaltic composition scattered over much of the world's ocean floors away from plate boundaries (e.g. Batiza, 1982), including the young (~ 6 Ma) 'Petit Spots' alkali basalts erupted on the 135 Ma Pacific plate (Hirano *et al.*, 2006). However, the melt mass produced (M_M) at any given location or region would be too small to build sizeable volcanic islands and island chains without sustained supply of fertile mantle material (M_{FM}) because of the relationship $M_M = F \times M_{FM}$. Therefore, scenario (1) cannot explain volumetrically significant OIB occurrences, but can explain widespread, yet volumetrically small, intra-plate seamounts that are far more in number than intra-plate volcanic islands (Craig & Sandwell, 1988; Wessel, 1997).

Obviously, scenario (2) satisfies the requirement for the F - P - L relationship and for production of sizeable (M_M) volcanic islands and island chains with a sustained supply of fertile mantle material (M_{FM}) from depth. In the absence of lithospheric extension to induce decompression melting, the deep mantle material beneath these intra-plate islands must rise dynamically as a consequence of its thermal or compositional buoyancy or both. Dynamic upwelling of the fertile mantle material leads to decompression melting. The 'dilution effect' discussed above suggests further that decompression melting starts in the garnet peridotite facies and continues to shallow levels in the spinel peridotite facies until the rising/melting mantle material is impeded by the lithospheric lid. This is an indirect, but important, line of evidence for decompression melting. Scenario (2) also explains the 'fixity' (relative to the faster moving plates) of many volcanically active oceanic islands. The Hawaiian Islands and the Hawaii-Emperor seamount chain provide the best example of this phenomenon. In fact, it was this observation that led to the use of the descriptive term 'hotspot' and the 'mantle plume' hypothesis (Wilson, 1963a, 1963b; Morgan, 1971,

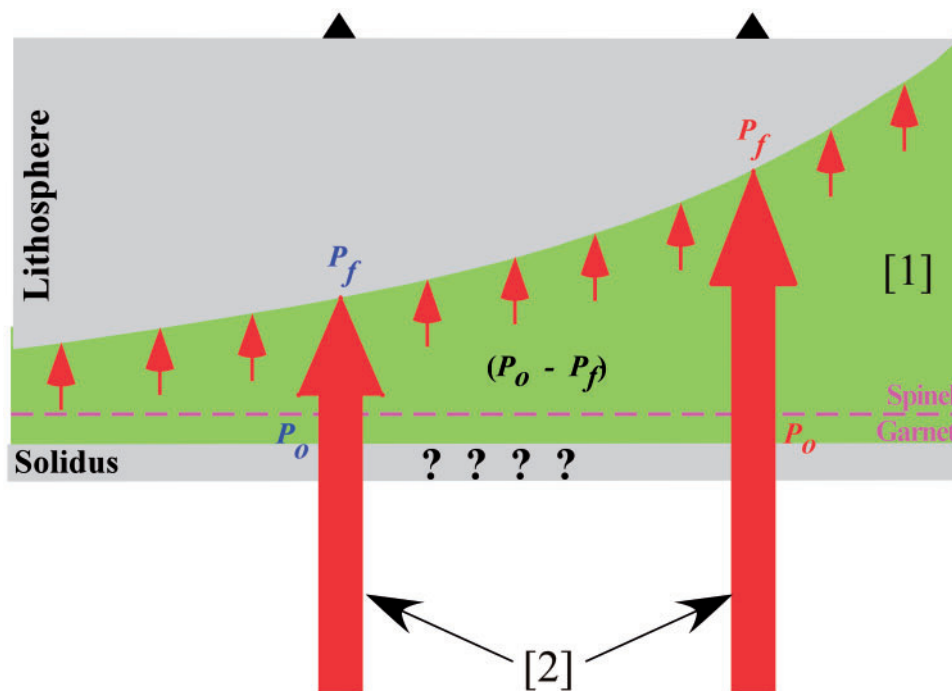


Fig. 6. A schematic illustration of two end-member scenarios to explain the lid effect on OIB geochemistry [i.e. $F \propto 1/L$ or $F \propto (P_o - P_f)$]: (1) sub-lid mantle ($P_o - P_f$) has a pervasive small melt fraction that has no lateral communication, otherwise melt mixing would eradicate the lid effect preserved in the OIB geochemistry; (2) columnar upwelling and decompression ($-\Delta P$) melting.

1972). Whether Hawaii-like OIB are indeed products of deep-rooted mantle plumes or shallow mantle melting anomalies sampling fertile mantle compositional heterogeneities has been a key issue of current plume debates (e.g. Davies, 2005; Foulger, 2005; Foulger *et al.*, 2005; Niu, 2005). The required dynamic upwelling from depth (Fig. 6), the relative fixity of intra-plate hotspots and the relative longevity of material supply together favour a 'mantle plume' origin for many intra-plate ocean islands and OIB petrogenesis. Nevertheless, the question remains as to whether these 'mantle plumes' do indeed initiate at the core–mantle boundary and whether the required buoyancy is purely thermal or thermal–chemical or both. We note that if the fertile source materials for OIB do not originate from the hot thermal boundary layer at the core–mantle boundary, it might be considered inappropriate to call these 'mantle plumes' according to Campbell & Davies (2006).

THE LID EFFECT ON OIB MINERAL CHEMISTRY

We have demonstrated above that oceanic lithosphere thickness variation, or the lid effect, exerts the primary control on OIB geochemistry on a global scale. It is thus expected that the phenocryst minerals that crystallize from OIB should also record the lid effect. Sobolev *et al.*

(2007) reported a high-quality dataset for the compositions (Ni, Cr, Mn, Ca as well as Fe and Mg) of olivine in basalts erupted at ocean ridges and in intra-plate settings with varying lithosphere thickness. These data are most consistent with the lid effect even though Sobolev *et al.* (2007) used these data as evidence to argue for the importance of 'recycled oceanic crust' (ROC) in the source regions of OIB and other intra-plate basaltic magmatism. Specifically, Sobolev *et al.* (2005, 2007) showed that olivine Ni contents are high in basalts erupted on thick (>70 km) lithosphere, low in basalts erupted on thin (<70 km) lithosphere, and lowest in MORB. This, plus the correlated variations of Cr, Mn and Ca in olivines allowed them to quantify that subducted oceanic crust (SOC) in the OIB source region is necessarily more abundant beneath thick lithosphere than beneath thin lithosphere. [Note: SOC is a description, but ROC is an interpretation that SOC is necessarily returned to OIB source regions.] They stated that the proportion of 'SOC-eclogite' in OIB mantle source regions increases with increasing lithosphere thickness (e.g. 5% beneath ocean ridges, 10% in Iceland mantle, and 20% in Hawaiian mantle). As a result, they proposed that 'SOC-eclogite-induced olivine-free pyroxenite' contributes more to the petrogenesis of the erupted basalts with increasing lithosphere thickness: ~10–20% for MORB, ~20% for Iceland 'OIB', ~40% for Detroit seamount OIB, ~60% for Hawaiian OIB and ~100% for Siberian flood

basalts. In making their arguments, Sobolev *et al.* (2005, 2007) used the Ni and Cr contents and Mn/Fe, Ni/Mg, Ni/(Mg/Fe) and Ca/Fe ratios in olivine. Below, we discuss these same parameters in the context of the lid effect.

The Niu & O'Hara (2007) interpretation

To use petrological and geochemical data effectively as a means to understand Earth processes, it is logical to look for possible correlations between petrological and geochemical parameters and physical observables. The first-order correlation between olivine phenocryst compositions and oceanic lithosphere thickness (Sobolev *et al.*, 2007) suggests a genetic link between the two. This led Niu & O'Hara (2007) to propose the lithosphere lid effect as the cause of the observed first-order olivine Ni variations. The left-hand panels of Fig. 7 are reproduced from the data of Sobolev *et al.* (2007). They show that at a given forsterite content (Fo), the olivine Ni content is conspicuously higher in OIB erupted on thick (>70 km) lithosphere (including Hawaii) than on thin (<70 km) lithosphere (including Iceland), and is higher than in MORB. Niu & O'Hara (2007) emphasized that this observation is consistent with the lid effect; that is, it is the product of the melting process rather than the original source composition. For example, for primitive olivines with Fo > 89, Ni_{THICK} (3417 ± 452 ppm, mean $\pm 1\sigma$, $N=1937$) > Ni_{THIN} (2477 ± 263 ppm, $N=746$) > Ni_{MORB} (2324 ± 296 ppm, $N=1700$) (see upper right panel of Fig. 7). Niu & O'Hara (2007) suggested that one of the simplest aspects of the lid effect is that melting beneath thick (>70 km) lithosphere is largely in the garnet peridotite facies through the melting reaction $a \text{ Cpx} + b \text{ Gnt} + c \text{ Ol} = 10 \text{ Melt} + d \text{ Opx}$ (Herzberg, 1992; Walter, 1998) where olivine, the primary Ni host, contributes to the melt. Melting beneath thin lithosphere occurs mostly in the spinel peridotite facies through melting reaction $a \text{ Cpx} + b \text{ Opx} + c \text{ Spl} = 10 \text{ Melt} + d \text{ Ol}$ (Baker & Stolper, 1994; Niu, 1997), where olivine crystallizes and sequesters Ni from the melt. As a result, high- P melting beneath thick lithosphere produces high-Ni melts whereas low- P melting beneath thin lithosphere produces low-Ni melts. Crystallization of these melts at crustal levels will produce high-Ni olivine from high- P melts erupted on thick lithosphere and low-Ni olivine from low- P melts erupted on thin lithosphere. Niu & O'Hara (2007) further suggested that a common peridotite source with Ni = 1900 ppm and ~10% melting can yield ~400 ppm and >560 ppm Ni in melts parental to MORB and those erupted on thick lithosphere, respectively. In support of the interpretation of Niu & O'Hara (2007), recent studies have shown that OIB olivine Ni contents can be readily explained without invoking the presence of significant recycled oceanic crust in the OIB source region (e.g. Li & Ripley, 2008, 2010; Wang & Gaetani, 2008; Matzen *et al.*, 2009; Putirka *et al.*, 2011).

The efficacy of the lid effect in explaining olivine compositions

The lid effect on OIB geochemistry is the effect of the final depth (pressure) of melting or melt equilibration (i.e. P ; see Figs 2 and 4). The efficacy of the lid effect in explaining OIB geochemistry means that it should also be able to explain the composition of olivines crystallized from OIB magmas provided that these olivines possess P -dependent properties or record P -dependent processes imparted from their parental melts. Our earlier discussion of olivine Ni contents hinted at the P -dependent properties of olivine and its parental melts.

We note that the abundances and ratios of trace and minor elements in olivine are a function of (1) their olivine/melt partitioning and (2) the inherited abundances and ratios of these elements from their parental melts. For example, the strong olivine/melt partitioning of Ni gives the high Ni content in olivine, but the latter is also proportional to the Ni content of the parental melt. These two variables must be considered when examining whether olivine chemistry in terms of Ni, Cr, Mn/Fe, Ni/Mg, Ni/(Mg/Fe) and Ca/Fe is P dependent and whether this P dependence is consistent with the lid effect. Using olivine Ni contents alone (i.e. considering $Kd_{\text{Ni}}^{\text{ol/melt}}$, including $Kd_{\text{Ni/Mg}}^{\text{ol/melt}}$ and $Kd_{\text{Ni/[Mg/Fe]}}^{\text{ol/melt}}$) to infer the Ni content in their parental melt and hence the pressure of melting or melt equilibration at mantle conditions is relatively straightforward because olivine is the most abundant mantle mineral stable at all depths of petrological interest (although advocates for olivine-free OIB sources would disagree), and, importantly, olivine is the primary host of Ni. Spinel is another Ni host (e.g. Liu *et al.*, 2008), but it is a minor phase stable only in the spinel peridotite facies, and is much less important for Ni. Elements such as Cr, Mn and Ca, as well as ratios such as Mn/Fe and Ca/Fe in the parental melts are controlled largely by other phases (spinel, garnet, opx and cpx as well as olivine to a lesser extent) during melting and melt equilibration under mantle conditions.

$$Kd_{\text{Ni}}^{\text{ol/melt}} = f(P)$$

There have been abundant olivine/melt partition coefficient data reported in the literature over the past 40 years, in particular since the systematic study of Hart & Davis (1978). However, experimental data on Fe-bearing system are limited and those obtained under high pressures even fewer (Seifert *et al.*, 1988; Herzberg & Zhang, 1996; Taura *et al.*, 1998; Filiberto *et al.*, 2009). Nevertheless, the limited dataset is adequate for our purpose; our interpretations can be made more quantitative in future as new data become available (e.g. Matzen *et al.*, 2009).

The existing data show that $Kd_{\text{Ni}}^{\text{ol/melt}}$ is non-linearly and inversely related to MgO in the melt, T and P

Compositions of liquidus olivines in mantle derived melts
(Sobolev *et al.*, 2007)

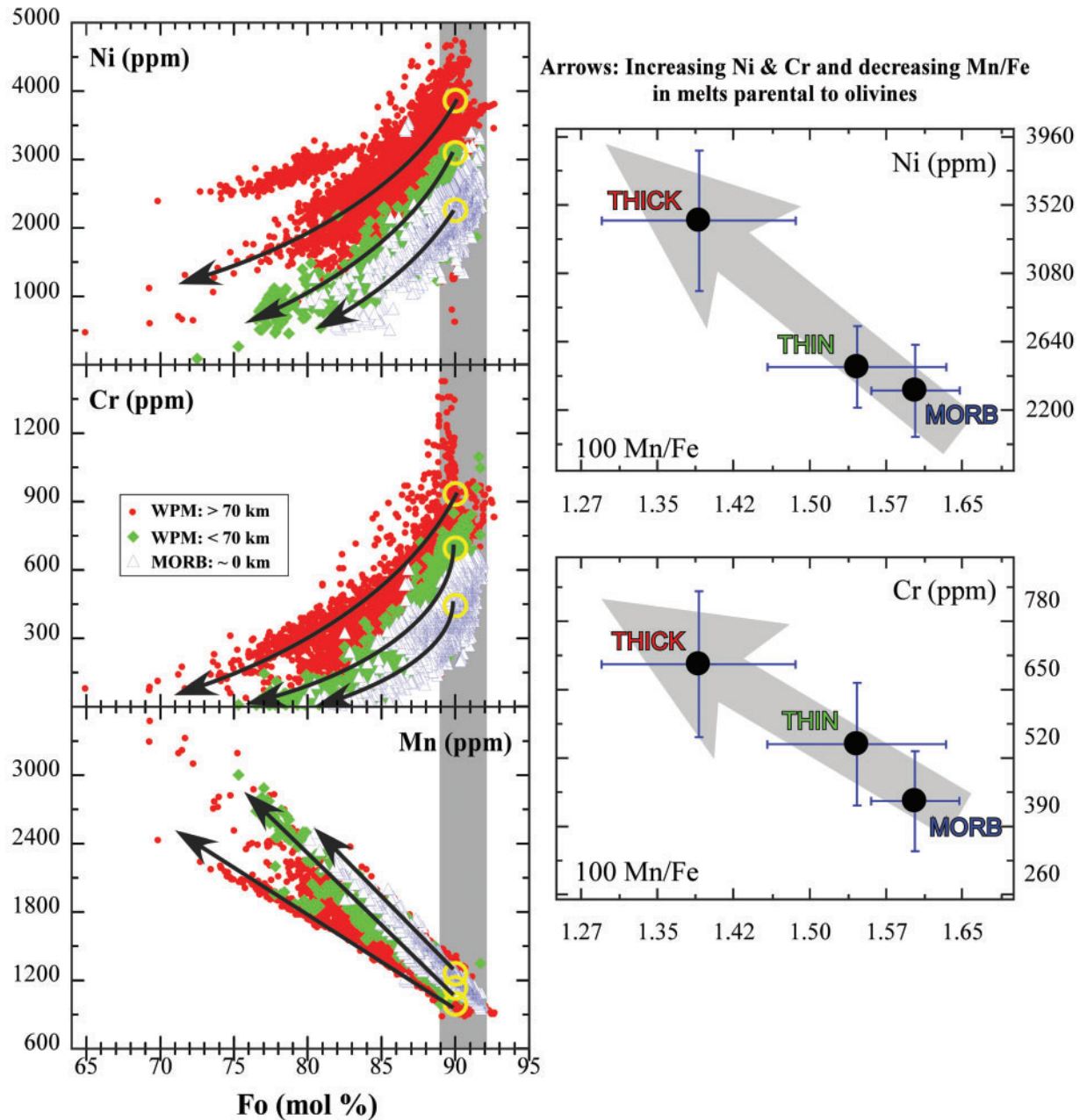


Fig. 7. The left panels are reproduced from the high-quality olivine data of Sobolev *et al.* (2007), who grouped samples in terms of ‘within-plate magmas’ erupted on thick (>70 km; WPM-THICK) and thin (<70 km; WPM-THIN) lithosphere and erupted at ocean ridges (MORB). The thick lines with arrows are approximate fractionation trends. The vertical gray band represents a subset of samples with olivine Fo > 89, which are used to calculate the averages for the three groups: $N=1937$ for WPM-THICK, 746 for WPM-THIN and 1700 for MORB. Two panels on the right plot these averages with $\pm 1\sigma$ in terms of Ni and Cr (ppm) vs 100Mn/Fe. 100Mn/Fe is a parameter used by Sobolev *et al.* (2007).

(e.g. Hart & Davis, 1978; Taura *et al.*, 1998; also see Fig. 8). As the liquidus T is positively correlated with MgO in the melt and because MgO contents in primary melts produced in peridotite melting experiments necessarily increase with both increasing T and P , it is thus not

straightforward to isolate the effects of P , T and melt composition (i.e. MgO). On the other hand, higher- P peridotite melting can only produce higher-MgO melts, and higher- P melting cannot occur without having higher T (i.e. solidus constraint). Therefore, to isolate these factors

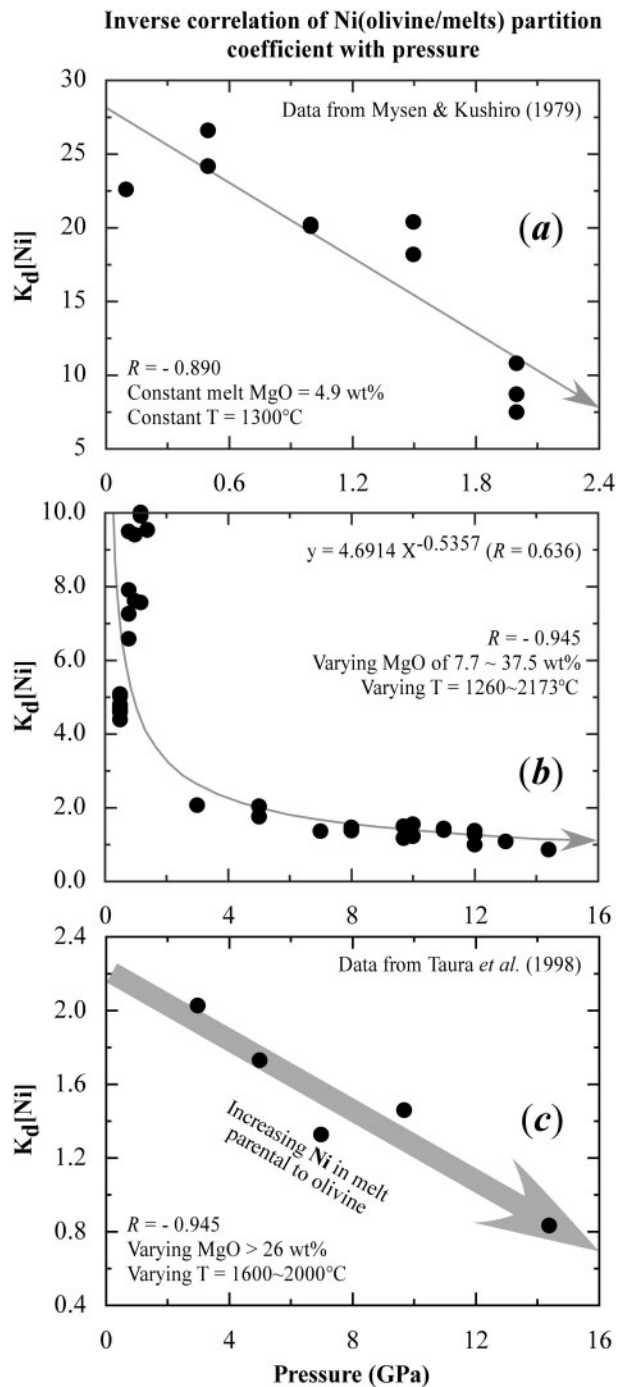


Fig. 8. High-pressure experimental data from the literature for Ni partition coefficient between olivine and silicate melt. (a) Data by Mysen & Kushiro (1979) on an Fe-free andesitic system. These data may not be used for natural systems, but they are ideal to show the inverse relationship because both $T = 1300^\circ\text{C}$ and $\text{MgO} = 4.9 \text{ wt } \%$ in the melt were kept constant in all runs. (b) A compilation of high- P data (Seifert *et al.*, 1988; Herzberg & Zhang, 1996; Taura *et al.*, 1998; Wang & Gaetani, 2008; Filiberto *et al.*, 2009). A power-law equation fits the data well. The huge K_d decrease with increasing P is probably the result of the combined effect of T , P and MgO in the melt as discussed in the text. [Note the data gap (or ‘rarity’) at $P \sim 1.5$ to 4 GPa.] (c) A subset of the data in (b) by Taura *et al.* (1998) that is

is unnecessary in practice because they intrinsically work together. This analysis is important for understanding the data for actual OIB and petrological processes. Nevertheless, Fig. 8a demonstrates explicitly that $K_{\text{Ni}}^{\text{ol/melt}}$ is a function of pressure (an inverse relationship) at constant T and MgO in the melt.

We also know that Ni contents in mantle-derived melts increase with increasing MgO (e.g. Clarke & O’Hara, 1979; Budahn, 1986). Indeed, we can readily derive an empirical equation: $\text{Ni} = 2.9594\text{MgO}^{1.859}$ [where Ni is in ppm, and MgO in weight per cent; $N = 5624$, $R^2 = 0.875$ for OIB samples with $\text{SiO}_2 < 53 \text{ wt } \%$ from the GEOROC database (<http://georoc.mpch-mainz.gwdg.de/georoc/>)]. From this analysis alone, we can see that parental OIB melts with higher MgO erupted on thicker lithosphere with higher MgO (Fig. 1) will have higher Ni, and will crystallize olivines with higher Ni than OIB melts erupted on thinner lithosphere. Hence, the lid effect is straightforward. In this context, it is noteworthy that in an attempt to model mantle potential temperatures for single mantle plumes, Herzberg & Gazel (2009) derived ‘primary plume melts’ with $\text{MgO} = 15.12 \pm 0.32 \text{ wt } \%$ for Iceland and $18.90 \pm 1.06 \text{ wt } \%$ for Hawaii, respectively. If these reconstructions are correct, then Iceland ‘primary melts’ would have ~ 460 ppm Ni whereas Hawaiian ‘primary melts’ would have ~ 700 ppm Ni. This explains why Hawaiian lavas have high-Ni olivines whereas Iceland lavas have low-Ni olivines; this can be readily explained by the lid effect. It is also important to note that the comparison between Hawaii and Iceland is particularly demonstrative of the lid effect because these two localities are the most widely accepted as ‘true mantle plumes’ and because they represent extreme end-members in terms of lithosphere thickness—young and thin lithosphere beneath Iceland and mature and thick lithosphere beneath Hawaii.

Figure 8 shows the available experimental data for $K_{\text{Ni}}^{\text{ol/melt}}$ as a function of pressure; of particular importance are those given in panels (b) and (c) determined in multi-component natural systems. Although there is an obvious data gap between $P \sim 1.5$ and 4 GPa, the inverse correlation of $K_{\text{Ni}}^{\text{ol/melt}}$ with increasing pressure is significant at all pressures, including, predictably, the data gap pressure range, for which better constrained experiments are needed (e.g. Matzen *et al.*, 2009). We can state with confidence that Ni increases in mantle-derived melts with

particularly dedicated to determining partitioning of transition metals between olivine and silicate melt at high pressures (see text). Again, an inverse $1/P$ relationship is significant. The grey arrow indicates the direction of increasing Ni in ‘primary’ mantle melts parental to the high-Ni olivines. It should be noted that each of the five data points from the Taura *et al.* (1998) experiments is an average of runs under the same pressures (i.e. 3 GPa = average of runs KLN-22 and 28 at 3 GPa; 5 GPa = average of runs KLB-15, 17, 20 and 23 at 5 GPa; 7 GPa = average of runs KLM-13 and 25 at 7 GPa; 9.7 GPa = average of runs KLB-31 and 35 at 9.7 GPa; 14.4 GPa = only one run KLN-43 at this pressure).

increasing pressure of melting or final depth of melt equilibration under mantle conditions. As a result, mantle melts with high- P signatures (Fig. 1) such as OIB erupted on thick lithosphere should have high Ni (e.g. Hawaiian lavas). Crystallization of these high-Ni melts will produce high-Ni olivines as seen in Hawaiian lavas (Sobolev *et al.*, 2005, 2007). In contrast, mantle melts with low- P signatures (Fig. 1) such as 'OIB' erupted on thin lithosphere should have low Ni contents (e.g. Iceland lavas). Crystallization of these low-Ni melts will produce low-Ni olivines as seen in Iceland lavas (e.g. Sobolev *et al.*, 2007). This P -dependent systematics in terms of $K_d^{\text{ol/melt}}$ is indicated by the arrowed lines (regression lines) in Fig. 8, where Fig. 8c is a close-up of the lower portion of Fig. 8b, which point in the direction of increasing Ni in mantle melts parental to olivines whose Ni content, in turn, is indicative of the pressure of melting and/or melt equilibration in the mantle. The P -dependent systematics of $K_d^{\text{ol/melt}}$ and $K_d^{\text{ol/melt}}$ in Fig. 9 have the same significance as $K_d^{\text{ol/melt}}$ in terms of P -dependent olivine control on Ni in mantle melts and in olivines crystallized from mantle melts because of the greater P -dependence of $K_d^{\text{ol/melt}}$ than $K_d^{\text{ol/melt}}$, $K_d^{\text{ol/melt}}$ and $K_d^{\text{ol/melt}}$ (Taura *et al.*, 1998), and because Ni is in the numerator in these ratio parameters.

Therefore, it is straightforward why olivines in lavas erupted on thicker lithosphere have higher Ni than olivines in lavas erupted on thinner lithosphere (Fig. 7; Niu & O'Hara, 2007).

$$K_d^{\text{ol/melt}} = f(P) \text{ and } \text{Bulk}D_{\text{Cr}}^{\text{solid/melt}} = f(P)$$

Experimental data, in particular high- P data on $K_d^{\text{ol/melt}}$, are few. The top two panels in Fig. 9 show a clear inverse relationship of $K_d^{\text{ol/melt}}$ with P . Like Ni, this would suggest that during melting Cr increases in the melt with increasing pressure because Cr becomes more incompatible in olivine (note $K_d^{\text{ol/melt}}$; Fig. 9). This would be consistent with the lid effect in that higher- P melts erupted on thicker lithosphere would have higher Cr and thus crystallize higher-Cr olivines than lower- P melts erupted on thinner lithosphere (Fig. 7). Although this apparent consistency favors the lid effect, this interpretation is only suggestive and incomplete. This is because olivine is not an important host for Cr, but rather Cr is largely hosted in spinel and to lesser extent in garnet and pyroxenes.

The lack of high-quality data on Cr partitioning between mantle minerals and basaltic melts at high- P conditions (see GERM K_d database: <http://earthref.org/cgi-bin/er.cgi?s=kdd-s0-main.cgi>) makes it difficult to properly evaluate $D_{\text{Cr}}^{\text{solid/melt}} = f(P)$ and thus the effect on the Cr content in the melt as a function of pressure. However, because spinel is the most important Cr host in mantle peridotite that is stable only in the spinel peridotite facies, and significantly more so than garnet and pyroxenes, and because spinel is not consumed during melting, but becomes more Cr rich as shown experimentally (e.g.

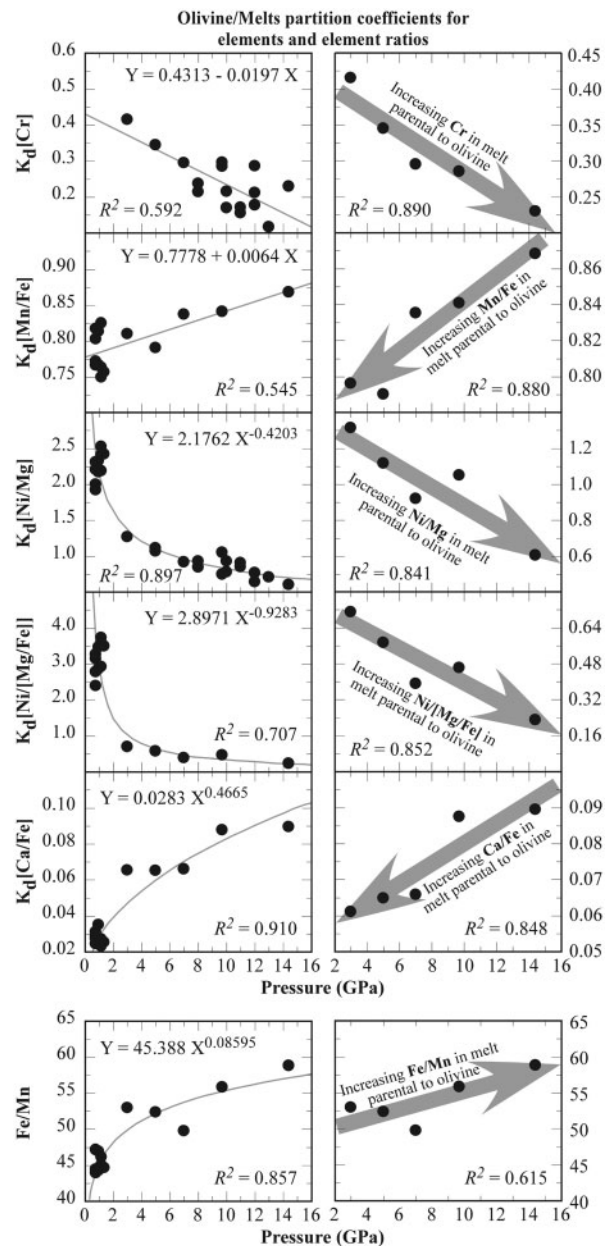


Fig. 9. The top 10 panels show plots of experimental data (the same source as in Fig. 10b and c) for partition coefficients of relevant elements or element ratios between olivine and silicate melt as a function of pressure. It should be noted that data runs that use an Fe (and Fe-wüstite) buffer are not used in panels that involve Fe. Panels on the left include all data when available, and panels on the right use the subset by Taura *et al.* (1998). Bottom two panels show Fe/Mn elemental ratios in the melt from the same experimental data plotted as a function of pressure.

Jaques & Green, 1980; Baker & Stolper, 1994) and observed in abyssal peridotites (e.g. Dick *et al.*, 1984; Dick, 1989; Niu & Hekinian, 1997b; Niu, 2004), it is thus apparent that melt produced in the garnet peridotite facies will have high Cr whereas melt produced in the spinel peridotite facies will have low Cr because Cr is preferentially held in

the residual Cr-spinel. This is consistent with the demonstration based on limited experimental data that $BulkD_{Cr}^{solid/melt} \propto 1/P$, and $BulkD_{Cr/Al}^{solid/melt}$ decreases with increasing melting pressure from the conditions of the spinel peridotite facies to the garnet peridotite facies as a result of the strong spinel (vs garnet and pyroxenes) control on Cr (see Canil, 2004). Therefore, higher- P OIB melts erupted on thicker lithosphere will have higher Cr and thus crystallize olivines with higher Cr than lower- P melts erupted on thinner lithosphere, which is the lid effect (see Fig. 7).

$$Kd_{[Mn/Fe]}^{ol/melt} = f(P) \text{ and } BulkD_{[Mn/Fe]}^{solid/melt} = f(P)$$

The similar geochemical behaviour of Fe and Mn in magmatic processes and the essentially constant Fe/Mn ratio of 60 ± 10 in a global peridotite survey (McDonough & Sun, 1995) suggest that Fe and Mn do not fractionate from each other in most magmatic processes, although a lower and more or less constant Fe/Mn ratio of 53.1 ± 4.6 has been observed in a large MORB glass dataset (see Niu & O'Hara, 2009). This perception had not encouraged analytical improvement of Mn until the study by Humayun *et al.* (2004), who showed varying Fe/Mn in different OIB suites and MORB. This is an important piece of work that alerted us to the necessity of obtaining improved Mn analyses. The olivine Mn analyses by Sobolev *et al.* (2007) are of high quality (Fig. 7). As those workers used the Mn/Fe ratio (or $100 \times \text{Mn/Fe}$) rather than Mn in their discussion, we thus use Mn/Fe accordingly for comparison.

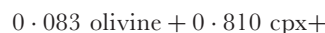
The obvious $Kd_{[Mn/Fe]}^{ol/melt}$ increase with increasing pressure (Fig. 9) is consistent with high- P melts having low Mn/Fe (or high Fe/Mn) and low- P melts having high Mn/Fe (or low Fe/Mn). However, this inference is again only suggestive because Mn is controlled not only by olivine, but also by pyroxenes, garnet and spinel during mantle melting, and because garnet and pyroxenes are known to fractionate Fe from Mn through peridotite melting experiments (see data compilation by Humayun *et al.*, 2004; Liu *et al.*, 2008). Therefore, a careful analysis is warranted. Nevertheless, it is convincing already from the same experimental data that the Fe/Mn ratio in the melt (bottom two panels of Fig. 9) increases with increasing pressure, but we can see only a very weak Fe/Mn increase with increasing lithosphere thickness (see Electronic Appendix Fig. A1), which, we feel, largely results from analytical uncertainties for Mn as a minor element of 'unknown petrological significance' accumulated over the past decades in the GEOROC database (<http://georoc.mpch-mainz.gwdg.de/georoc/>). For example, using improved analytical techniques (inductively coupled plasma mass spectrometry), Humayun *et al.* (2004) reported Fe/Mn = 66.6 ± 0.6 for Hawaiian picritic melts, 59.5 ± 1.5 for Iceland picritic melts, and 56.5 ± 1.1 for MORB (an existing larger dataset on MORB gives a lower value of Fe/Mn = 53.1 ± 4.6 ; Niu & O'Hara, 2009). It should be noted also that using the

more recent analyses and in an attempt to reconstruct 'primary plume' melts, Herzberg & Gazel (2009) arrived at Fe/Mn = 67.35 ± 2.99 for Hawaii and 57.64 ± 1.56 for Iceland. These observations are consistent with the lid effect (Fig. 7); that is, higher- P OIB melts erupted on thicker lithosphere (e.g. Hawaiian case) with higher Fe/Mn will crystallize olivines with higher Fe/Mn (or lower Mn/Fe or Mn at a given Fo) than lower- P OIB melts erupted on thinner lithosphere (e.g. Iceland case), and than MORB (see Fig. 7).

The question is why $BulkD_{[Mn/Fe]}^{solid/melt}$ is proportional to P . Figure 9 shows that $Kd_{[Mn/Fe]}^{ol/melt} \propto P$, but we must consider other phases as well during mantle melting. The answer lies in the peridotite melting experiments shown in Fig. 10a. There is no doubt that some significant analytical errors exist for Mn in these experimental data because of the difficulties in analysing such once under-utilized minor elements; however, the distinctive $Kd_{[Mn/Fe]}$ values for olivine, opx, cpx and garnet are likely to be real (note: $Kd_{[Mn/Fe]} = Kd_{[Mn]}/Kd_{[Fe]}$ mathematically). Because there is no obvious variation in these values with increasing pressure, we can consider the averages given at the top right corner of Fig. 10a. These average values are expected, statistically, to have largely averaged out analytical and other uncertainties.

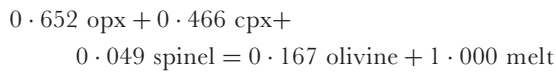
We concluded above that OIB are produced by decompression melting of dynamically upwelling fertile mantle material beginning in the garnet peridotite facies and continuing into the spinel peridotite facies until the upwelling stops, limited by the lithosphere lid. We also concluded that OIB geochemistry reflects a mixture of melts produced in both the garnet and spinel peridotite facies, and that the low- F melt signature (i.e. highly enriched in incompatible elements and the 'garnet' signature) is diluted as a result of continued melting in the spinel peridotite facies. It is diluted less beneath thick lithosphere (e.g. high $[La/Sm]_N$ and $[Sm/Yb]_N$ in Fig. 1) and is diluted more beneath thin lithosphere (e.g. low $[La/Sm]_N$ and $[Sm/Yb]_N$ in Fig. 1) because the extent of melting is controlled by the lithospheric lid and increases with decreasing lithosphere thickness. This allows us to evaluate melting in the garnet and spinel peridotite facies separately to have a clearer understanding of the Mn/Fe behaviour during melting. Because mantle melting is incongruent in both the garnet peridotite facies (e.g. Herzberg, 1992; Walter, 1998) and the spinel peridotite facies (Baker & Stolper, 1994; Niu, 1997), we consider the following melting reactions.

- (1) Incongruent melting reaction in the garnet peridotite facies; Walter (1998):



(initial modes: 0.53 olivine, 0.27 cpx, 0.04 garnet and 0.16 opx).

- (2) Incongruent decompression melting ‘reaction’ in the spinel peridotite facies derived from abyssal peridotite data by Niu (1997):



(Initial modes: 0.513 olivine, 0.341 opx, 0.131 cpx and 0.015 spinel).

Using the $Kd_{[\text{Mn}/\text{Fe}]}$ value in Fig. 10a, and by assuming $Kd_{[\text{Mn}/\text{Fe}]}$ for spinel (very minor, only ~1.5 wt %) is the same as for olivine, we obtained the following (see Zou, 2000):

$$D_O : D_{\text{garnet facies}}^{[\text{Mn}/\text{Fe}]} = 1.136 > D_{\text{spinel facies}}^{[\text{Mn}/\text{Fe}]} = 1.065 (6.6\% \text{ higher})$$

$$P_O : P_{\text{garnet facies}}^{[\text{Mn}/\text{Fe}]} = 1.607 > P_{\text{spinel facies}}^{[\text{Mn}/\text{Fe}]} = 1.383 (16.2\% \text{ higher})$$

$$Q_O : Q_{\text{garnet facies}}^{[\text{Mn}/\text{Fe}]} = 1.673 > Q_{\text{spinel facies}}^{[\text{Mn}/\text{Fe}]} = 1.480 (13.1\% \text{ higher})$$

where D_o is the initial bulk distribution coefficient, P_o is the bulk distribution coefficient owing to melting phases on the left-hand side of the reactions, and Q_o is the effective bulk distribution coefficient including the effect of the crystallization phase on the right-hand side of the reactions (opx or olivine). These simple calculations illustrate that the Mn/Fe ratio is ‘compatible’ during mantle melting and is more ‘compatible’ during melting in the garnet peridotite facies than in the spinel peridotite facies. As a result, melt produced in the garnet peridotite facies will have low Mn/Fe (i.e. high Fe/Mn) whereas melt produced in the spinel peridotite facies will have high Mn/Fe (i.e. low Fe/Mn). These are the two end-member scenarios, and continued decompression melting from the garnet peridotite facies through the spinel peridotite facies will have an end-product between these because of the ‘dilution effect’ or the geochemically ‘melting-induced’ mixing effect (see above).

All the above analyses are consistent with a statement that with increasing pressure of melting or melt equilibration under mantle conditions, Ni, Cr and Fe/Mn (vs Mn/Fe) in the melt increase. That is, high- P melts have high Ni and Cr and low Mn/Fe, whereas low- P melts have low Ni and Cr and high Mn/Fe. Crystallization of these melts at shallow levels will produce olivines with high Ni and Cr and low Mn/Fe from high- P melts erupted on thick lithosphere and olivines with low Ni and Cr and high Mn/Fe from low- P melts erupted on thin lithosphere. This is shown graphically on the two panels on the right in Fig. 7, where the arrows point in the direction of increasing pressure of melting or melt equilibration of mantle conditions. This is again the lid effect.

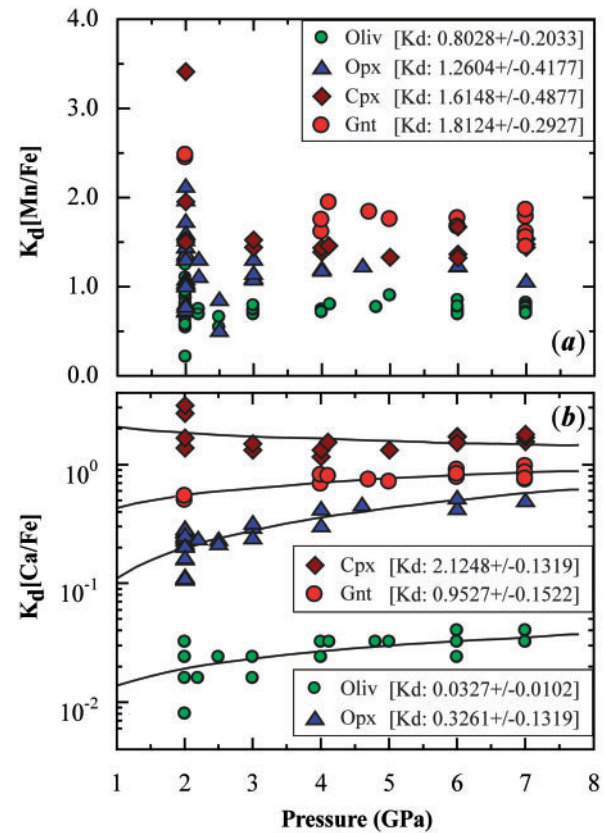


Fig. 10. (a) Partition coefficient ratios of Mn/Fe extracted from peridotite melting experiments with $P \geq 2$ GPa. Data were compiled by Liu *et al.* (2008) from Takahashi & Kushiro (1983), Hirose & Kushiro (1993), Gaetani & Grove (1998), Walter (1998), Falloon & Danyushevsky (2000) and Parman & Grove (2004). There is no obvious $Kd_{[\text{Mn}/\text{Fe}]}$ change as a function of pressure, but each of the four phases show distinctive values: garnet 1.812, Cpx 1.615, Opx 1.260 and olivine 0.803. No $Kd_{[\text{Mn}/\text{Fe}]}$ is reliably available for spinel, but a similar value to that of olivine may be used by assuming spinel does not fractionate Fe and Mn significantly. (b) Partition coefficient ratio of Ca/Fe from the same experimental data as in (a). Except for a few runs at 2 GPa for Cpx, all the data for each of the four phases show a systematic $Kd_{[\text{Ca}/\text{Fe}]}$ increase with increasing pressure. The curves are power-law fits.

A comment on the significance of Fe/Mn in basaltic rocks

We have shown above that high Fe/Mn is a likely characteristic of melt produced in the garnet peridotite facies or largely so (e.g. Hawaiian lavas) whereas low Fe/Mn is more typical of melting in the spinel peridotite facies (e.g. MORB). It should be noted, however, that high Fe/Mn is not a simple echo of the familiar ‘garnet signature’ defined by heavy REE depletion or elevated $[\text{Sm}/\text{Yb}]_{\text{PM}}$ (Fig. 1), but a more complex effect of incongruent melting involving not only garnet, but also pyroxenes, in particular opx, which is a crystallizing phase and retains Mn (i.e. $Kd_{\text{opx}}^{[\text{Mn}/\text{Fe}]} = 1.26$) during melting and in the residue (see above). This Fe/Mn argument, along with olivine Ni, Cr and all other OIB geochemical systematics (Fig. 1), argues

convincingly that the lid effect is rather significant on a global scale. This is not surprising at all in terms of straightforward physics because the oceanic lithospheric lid thickness varies so much from <20 km to ~90 km (see above). However, Humayun *et al.* (2004) interpreted the high Fe/Mn of Hawaiian lavas in terms of the excess Fe in a Hawaiian plume derived from the core–mantle boundary with excess Fe input from the outer core. Following Sobolev *et al.* (2005, 2007), many have attempted to explain the presence of high-Ni olivine in some continental basalts as resulting from an olivine-free pyroxenite source produced by interaction of harzburgite with a SiO₂-rich melt of recycled oceanic or continental crust (e.g. Gao *et al.*, 2008; Liu *et al.*, 2008; Zhang *et al.*, 2009). We suggest that (1) caution is necessary when proposing such interpretation; (2) Fe/Mn in basalts can be a useful indicator of pressure of melting in terms of relative melt contributions from the garnet or spinel peridotite facies; this may be particularly useful for interpreting the petrogenesis of basalts in continental settings where lithospheric thickness variations may be of geodynamic significance; (3) Fe/Mn variations can also be caused by fertile source compositional variations or crustal level contamination (e.g. in the case of Mn-rich sediments); (4) there is a need to obtain high-quality Mn analyses in future geochemical studies of OIB.

$$Kd_{[Ca/Fe]}^{ol/melt} = f(P) \text{ and } BulkD_{[Ca/Fe]}^{solid/melt} = f(P)$$

Figure 9 shows that $Kd_{[Ca/Fe]}^{ol/melt}$, as does $Kd_{[Mn/Fe]}^{ol/melt}$, increases with increasing pressure although the latter is much greater. This suggests that a positive co-variation should exist between Ca/Fe and Mn/Fe in olivines if their parental melt compositional differences reflect pressure differences. Experimental studies and modelling efforts show that CaO in mantle melts is inversely (weakly) related to pressure of melting whereas FeO in the melt is positively related to the pressure of melting (e.g. Jaques & Green, 1980; Niu & Batiza, 1991; Walter, 1998). Hence, melts parental to high Ca/Fe olivines from OIB erupted on thin lithosphere are of low-*P* origin with high CaO/FeO, whereas melts parental to low Ca/Fe olivines from OIB erupted on thick lithosphere are of high-*P* origin with low CaO/FeO. This is again the lid effect. It is readily shown in Fig. 10b that mineral/melt $Kd_{[Ca/Fe]}$ values increase with increasing pressure for olivine, opx and garnet. This is also true for cpx except for four runs at 2.0 GPa (Fig. 10b).

OIB olivine data favor the lid effect, rather than varying proportion of recycled oceanic crust in mantle source regions

The left-hand panels in Fig. 11 are reproduced from Sobolev *et al.* (2007) with our added gray arrows. Sobolev *et al.* proposed that the compositions of olivines crystallized from peridotite-derived melts have high Mn/Fe and Ca/Fe, but low Ni/Mg and Ni/[Mg/Fe], whereas the compositions of olivines crystallized from olivine-free

pyroxenite-derived melts have low Mn/Fe and Ca/Fe, but high Ni/Mg and Ni/[Mg/Fe]. The olivine-free pyroxenite source was inferred to result from interaction of harzburgite with a SiO₂-rich melt derived from recycled oceanic crust (ROC). Therefore, the compositional variation of olivines in MORB, in OIB erupted on thin lithosphere and in OIB erupted on thick lithosphere could reflect parental melts with increased proportions of pyroxenite-derived melt as a result of an increasing ROC proportion in the mantle source regions beneath ocean ridges, thin lithosphere and thick lithosphere respectively. The right-hand panels in Fig. 11 demonstrate that the olivine compositional variation is simply a consequence of the lid effect without the need to invoke varying proportions of ROC. The OIB olivine dataset of Sobolev *et al.* (2007) provides additional evidence in support of oceanic lithospheric thickness control on OIB geochemistry.

ON THE CONSTANT THICKNESS OF THE MATURE OCEANIC LITHOSPHERE

The bottom of the seismic low-velocity zone (LVZ) beneath the ocean basins is at about 220 km depth (Anderson, 1995), whereas the top is determined by the thickness of the lithospheric lid. Conductive heat loss or thermal contraction can explain both the ocean depth (first order) and lithosphere thickness as a function of lithosphere age [i.e. $L = 11 t^{0.5}$, or the half-space cooling model (HSM)]. However, the HSM explains only the lithosphere thickness formed in the first ~70 Myr, after which the lithosphere maintains a constant thickness of ~90 km. There is no obvious reason why the lithosphere should stop thickening as heat loss continues after the first 70 Myr, which has led to much effort to explain this observation. Suggestions vary from ideas such as ‘lithosphere phase transitions’ (Wood & Yuen, 1983) to ‘mantle plume heating’ (Sleep, 1987; Davies, 1988), the instability of the deep lithosphere because of the ‘inevitable’ lithospheric small-scale convection (erosion) (e.g. Parson & McKenzie, 1978; Yuen & Fleitout, 1985; Huang & Zhong, 2005; Sleep, 2011), and the plate model (vs HSM; e.g. Stein & Stein, 1992). Nevertheless, the currently popular model of ‘small-scale convective erosion’ still requires heat supply against conductive heat loss to the seafloor (Huang & Zhong, 2005; Sleep, 2011). Hence, the problem remains unresolved.

This apparently perplexing physical or geophysical problem may actually be a petrological problem. On the basis of many experimental investigations into the petrogenesis of mantle-derived melts (Lambert & Wyllie, 1968, 1970; Green, 1971, 1991; Millhollen *et al.*, 1974; Wyllie & Huang, 1975; Wyllie, 1978, 1987, 1988*a*, 1988*b*; Wyllie *et al.*, 1983; White & Wyllie, 1992; Lee & Wyllie, 2000; Lee *et al.*,

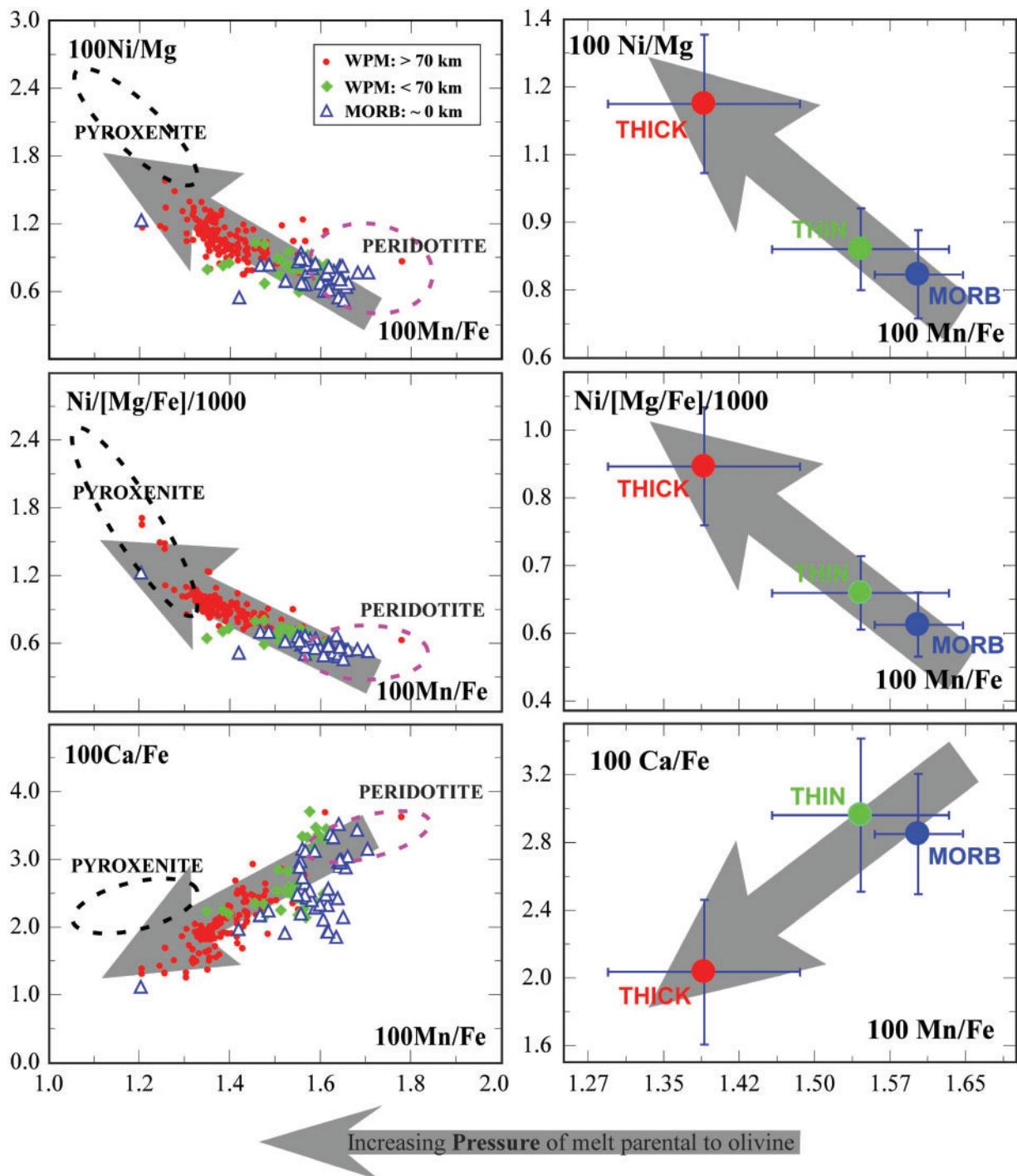


Fig. 11. Left panels are reproduced from Sobolev *et al.* (2007) with our added gray arrows. Sobolev *et al.* (2007) indicated their expected compositions of (1) olivines crystallized from peridotite-derived melts with high Mn/Fe and Ca/Fe, and low Ni/Mg and Ni/[Mg/Fe]; (2) olivines crystallized from olivine-free pyroxenite-derived melts with low Mn/Fe and Ca/Fe, and high Ni/Mg and Ni/[Mg/Fe]. Olivines from MORB (open triangles), OIB erupted on thin lithosphere (filled diamonds) and OIB erupted on thick lithosphere (filled circles) reflect parental melts with increased proportion of pyroxenite melt as a result of increased SOC in OIB source regions. The SOC abundances in OIB source regions increase with increasing lithosphere thickness. Right panels show our interpretation using average compositions of olivines with Fo > 89 (see Fig. 7) in terms of straightforward melting reactions in both garnet and spinel peridotite stability fields and experimentally well-constrained partition coefficients. As indicated, the arrows point to the direction of increasing pressure of melt equilibration under mantle conditions as a result of lithosphere thickness variation, which limits the final depth of melting; that is, the lid effect.

2000), Green and coworkers (Green, 1971; Green & Liebermann, 1976; Green & Falloon, 2005; Green *et al.*, 2010) suggested that the lithosphere-to-LVZ transition (equivalent to the LAB) may represent a petrological transition from subsolidus amphibole (pargasite)-bearing lherzolite (the lithosphere) to lherzolite containing a very small fraction of H₂O-rich melt (~1%; the LVZ). They placed the transition at ~90 km depth.

We considered above the base of the lithosphere (LAB) as a natural peridotite solidus (i.e. representing the depth of melting cessation for decompression melting; Niu & O'Hara, 2003, 2009) to explain petrological observations (e.g. Fig. 1), whereas it is defined geophysically as an isotherm. Indeed, the presence of a melt layer at or immediately below the oceanic LAB is required to explain the role of metasomatic source enrichment in the geochemistry of OIB and seamounts (Niu & O'Hara, 2003, 2009; Humphreys & Niu, 2009) and also the large (6–9%) shear-wave velocity drop (e.g. Kawakatsu *et al.*, 2009), consistent with the LAB being a peridotite solidus. Furthermore, Kawakatsu *et al.* (2009) and Kumar & Kawakatsu (2011) showed with modelling (using $T_p = 1315^\circ\text{C}$) that the LAB is most consistent with an isotherm of 1100°C . For both isotherm (1100°C) and solidus to 'coincide', the solidus must have a slope $dT/dP \sim 0$ in P - T space, which would be consistent with the pargasite (amphibole) dehydration solidus (near isothermal) of volatile-bearing mantle peridotite: H₂O-CO₂-peridotite (Fig. 5a) or H₂O-peridotite (Fig. 5b; Green *et al.*, 2010). In Fig. 5a, the 'wet' dehydration solidus becomes complex at depths of 70–90 km because of varying CO₂/H₂O ratios in various experiments (see Wyllie, 1988*b*, for review).

Because pargasite in volatile-bearing mantle peridotite is stable at $P \leq 3.0$ GPa (or ~90 km) and $T \leq 1100^\circ\text{C}$ (e.g. Green & Falloon, 1998, 2005), we infer that the correct pargasite dehydration solidus in the natural CO₂-H₂O-peridotite system should have the topology as indicated by the blue curve in Fig. 5a (Green & Falloon, 1998, 2005; Green *et al.*, 2010); however, well-constrained experiments for the H₂O-CO₂-peridotite system in the 2.5–4.0 GPa pressure range are needed to verify this. The straightforward and significant implications are as follows.

- (1) The stability of pargasite (and its dehydration solidus) determines the depth of the base of the oceanic lithosphere.
- (2) If $P < 3$ GPa ($< \sim 90$ km), the dehydration solidus is an isotherm ($dT/dP \approx 0$) of $\sim 1100^\circ\text{C}$ (Fig. 5a and b). Pargasite is stable (lithosphere) if $T < 1100^\circ\text{C}$, but is replaced by peridotite with incipient melt (asthenosphere) if $T > 1100^\circ\text{C}$ (Fig. 5b).
- (3) If $P \approx 3$ GPa (~ 90 km), the dehydration solidus is isobaric ($dP/dT \approx 0$) (Fig. 5a).
- (4) If $P > 3$ GPa ($> \sim 90$ km), mantle at this depth is within the asthenosphere with no pargasite, but

peridotite containing a small melt fraction. This latter observation is consistent with the requirement for a compositionally stratified LVZ of which the upper part close to the LAB is enriched in volatiles (required to stabilize pargasite) and incompatible elements whereas the lower part provides the depleted source for MORB (Niu & O'Hara, 2009).

The above analysis explains why the mature (>70 Ma) oceanic lithosphere cannot be thicker than 90 km without the need to invoke complex processes.

SUMMARY

- (1) Following Humphreys & Niu (2009), we have further averaged the global OIB geochemical dataset into 11 lithosphere thickness intervals each of 10 km with the aim of averaging out effects such as detailed OIB compositional variations within a single island, between islands, between island groups, and between ocean basins, as a result of fertile mantle compositional variation on all scales and different spreading histories of the oceanic lithosphere on which the intra-plate ocean islands are built. Such heavily averaged data should show first-order physical effects of lithosphere thickness variation on mantle melting and melt equilibrium processes.
- (2) Our results (Fig. 1) show explicitly that oceanic lithosphere thickness variation exerts a first-order control on the geochemistry of OIB, which is readily explained by the lid effect (Fig. 2). Variation in the initial depth of melting as a result of fertile mantle compositional variation and mantle potential temperature variation can influence OIB compositions, but these two variables must have secondary effects because they do not overshadow the effect of lithosphere thickness variation that is prominent on a global scale (Fig. 1).
- (3) Mantle melting beneath intra-plate volcanic islands must begin in the garnet peridotite facies, resulting in the familiar 'garnet signature' in all OIB samples (e.g. $[\text{Sm}/\text{Yb}]_N > 1$); however, this ratio decreases from ~5 beneath the thickest lithosphere to ~2 beneath thin lithosphere, suggesting a dilution effect by continued melting in the spinel peridotite facies as the lithosphere thickness decreases (Fig. 1). This dilution effect also applies to low- F melt signatures (i.e. elevated abundances of incompatible elements such as Ti and P and elemental ratios La/Sm (Fig. 1) and even radiogenic isotopes (Fig. 3)).
- (4) The dilution effect shown by radiogenic isotopes is consistent with our knowledge that the mantle source regions for oceanic basalts are heterogeneous, and

have, broadly speaking, two components: an 'ancient' enriched component with a low solidus temperature dispersed in the more refractory/depleted (or less enriched) matrix. Thus, the early stage low- F melt is dominated by this enriched component with elevated abundances of incompatible elements coupled with radiogenic isotopes. This enriched component in the melt is diluted progressively with continued decompression melting with decreasing lithosphere thickness or plate age (Figs. 3).

- (5) The significant correlations of OIB geochemical parameters (Figs 1 and 4) with lithosphere thickness suggest that the most reliable P - T condition recorded in OIB geochemistry is not the initial depth of melting (P_o) but the final depth of melting or melt equilibration (P_f) in the mantle as constrained by the thickness of the lithospheric lid. This suggests that basalt-based thermobarometry must be used with caution when inferring mantle potential temperatures (T_p) and solidus depths because OIB do not unequivocally record such information. Any attempt to do so requires proper correction for the lid effect.
- (6) The 'dilution effect' in (3) suggests that mantle melting beneath intra-plate volcanic islands takes place in the asthenosphere by decompression of dynamically ascending fertile source material rising from depth. Melting begins in the garnet peridotite facies and continues in the spinel peridotite facies until the rising/melting material reaches the base of the lithosphere. The dynamic ascent of the fertile OIB source material requires that the material is buoyant either because it is hotter or compositionally less dense (or both) than the ambient mantle. In either scenario, columnar upwelling beneath a single island group is the most logical explanation; whether we call such features 'plumes' or 'diapirs' (Fig. 5) will depend on proving whether they originate from the hot thermal boundary layer at the core-mantle boundary or from compositionally enriched heterogeneities embedded in the shallower mantle.
- (7) The compositions (e.g. Ni, Cr, Ni/Mg, Ni/[Mg/Fe], Mn/Fe and Ca/Fe) of olivine phenocrysts in OIB are wholly consistent with the lithosphere lid effect without the need to invoke varying proportions of SOC in the OIB source regions as a function of oceanic lithosphere thickness, which has many difficulties.
- (8) The Fe/Mn ratio in OIB is a useful parameter and is positively correlated with melt contributions from the garnet (vs spinel) peridotite facies. Hence, a high Fe/Mn ratio in basalts neither indicates a high proportion of SOC in the source region of the basalts nor suggests that the source regions have elevated Fe (vs

Mn) because of Fe contribution from the core in the case of Hawaiian 'plumes'.

- (9) The nature of the LAB (i.e. the base of the oceanic lithosphere) for plate ages <80 Ma is defined by the near-isothermal ($\sim 1100^\circ\text{C}$) pargasite dehydration solidus (i.e. the wet $\text{H}_2\text{O} + \text{CO}_2$ -peridotite system) with a melt layer present at or immediately below the LAB required to explain the geochemistry of OIB and seamounts and to explain the large shear-wave velocity drop
- (10) If the nature of the LAB is indeed controlled by the pargasite dehydration solidus, then the stability of this mineral under conditions of $T \leq 1100^\circ\text{C}$ and $P \leq 3.0$ GPa suggests that the constant lithosphere thickness (i.e. no thicker than ~ 90 km) for older (>70 Ma) oceanic lithosphere may actually be a simple petrological problem without having to invoke complex processes.

ACKNOWLEDGEMENTS

It is our great pleasure to contribute to this special issue in honour of Peter J. Wyllie for his life-long dedication and numerous significant scientific contributions to our better understanding how the Earth works by means of experimental petrology. Y.N. thanks Pete for his friendship, encouragement and enjoyable scientific exchanges over the years, and for his profound influence in research philosophy. Discussion with many colleagues over the years have been helpful, including Francis Albarède, Don Anderson, Pat Castillo, David Clague, Geoff Davies, Henry Dick, Godfrey Fitton, Gillian Foulger, Fred Frey, Dave Green, Karsten Haase, Claude Herzberg, Al Hofmann, Cin-Ty Lee, Shuguang Li, Yan Liang, Caroline Lithgow-Bertelloni, Bill McDonough, Jim Natland, Sebastian Pilet, Dean Presnall, Marcel Regelous, Vincent Salters, Alex Sobolev, Lars Stixrude, Ed Stolper, Bill White, Peter Wyllie, Yi-gang Xu and Youxue Zhang. We thank Ian Campbell, Keith Putirka and Vincent Salters, and Editor Gerhard Wörner, for their constructive comments, which have helped to improve the paper.

FUNDING

Y.N. thanks the Leverhulme Trust for a Research Fellowship, Durham University for a Christopherson/Knott Fellowship, China University of Geosciences in Beijing and Peking University for visiting Professorships in the preparation of the paper. This work is partially supported by the Chinese 111 Project (No. B07011) and Chinese NSF (No. 91014003).

SUPPLEMENTARY DATA

Supplementary data for this paper are available at *Journal of Petrology* online.

REFERENCES

- Anderson, D. L. (1995). Lithosphere, asthenosphere, and perisphere. *Reviews of Geophysics* **33**, 125–149.
- Anderson, D. L. (2011). Hawaii, boundary layers and ambient mantle—geophysical constraints. *Journal of Petrology* **52**, 000–000.
- Baker, M. B. & Stolper, E. M. (1994). Determining the composition of high-pressure mantle melts using diamond aggregates. *Geochimica et Cosmochimica Acta* **58**, 2811–2827.
- Batiza, R. (1982). Abundances, distribution and sizes of volcanoes in the Pacific Ocean and implications for the origin of non-hotspot volcanoes. *Earth and Planetary Science Letters* **60**, 195–206.
- Batiza, R. & Vanko, D. A. (1984). Petrology of young Pacific seamounts. *Journal of Geophysical Research* **89**, 11235–11260.
- Budahn, J. R. (1986). Evidence for equilibrium conditions during the partitioning of nickel between olivine and komatiite liquids. *American Mineralogist* **71**, 1337–1342.
- Campbell, I. H. (2005). Large igneous provinces and the mantle plume hypothesis. *Element* **1**, 265–270.
- Campbell, I. H. & Davies, G. F. (2006). Do mantle plumes exist? *Episodes* **29**, 162–168.
- Campbell, I. H. & Griffiths, R. W. (1990). Implications of mantle plume structure for the evolution of flood basalts. *Earth and Planetary Science Letters* **99**, 79–83.
- Canil, D. (2004). Mildly incompatible elements in peridotites and the origins of mantle lithosphere. *Lithos* **77**, 375–393.
- Castillo, P. R. & Batiza, R. (1989). Strontium, neodymium and lead isotope constraints on near-ridge seamount production beneath the South Atlantic. *Nature* **342**, 262–265.
- Castillo, P. R., Natland, J. H., Niu, Y. L. & Lonsdale, P. (1998). Sr, Nd, and Pb isotopic variation along the Pacific ridges from 53 to 56°S: Implications for mantle and crustal dynamic processes. *Earth and Planetary Science Letters* **154**, 109–125.
- Castillo, P. R., Klein, E., Bender, J., Langmuir, C., Shirey, S., Batiza, R. & White, W. (2000). Petrology and Sr, Nd, and Pb isotope geochemistry of mid-ocean ridge basalt glasses from the 11°45'N to 15°00'N segments of the East Pacific Rise. *Geochemistry, Geophysics, Geosystems* **1**, 1999GC000024.
- Castillo, P. R., Clague, D. A., Davis, A. S. & Lonsdale, P. F. (2010). Petrogenesis of Davidson Seamount lavas and its implications for fossil spreading center and intraplate magmatism in the eastern Pacific. *Geochemistry, Geophysics, Geosystems* **11**, doi:10.1029/2009GC002992.
- Clarke, D. B. & O'Hara, M. J. (1979). Nickel, and the existence of high-MgO liquids in nature. *Earth and Planetary Science Letters* **44**, 153–158.
- Craig, C. H. & Sandwell, D. T. (1988). Global distribution of seamounts from Seasat profiles. *Journal of Geophysical Research* **93**, 10408–10420.
- Davies, G. F. (1988). Ocean bathymetry and mantle convection: I. Large scale flow and hotspots. *Journal of Geophysical Research* **93**, 10467–10480.
- Davies, G. F. (1999). *Dynamic Earth: Plates, Plumes and Mantle Convection*. Cambridge University Press: Cambridge, 460 p.
- Davies, G. F. (2005). A case for mantle plumes. *Chinese Science Bulletin* **50**, 1541–1554.
- Dick, H. J. B. (1989). Abyssal peridotites, very slow spreading ridges and ocean ridge magmatism. In: Saunders, A. D. & Norry, M. J. (eds) *Magmatism in the Ocean Basins*. Geological Society, London, *Special Publications* **42**, 71–105.
- Dick, H. J. B., Fisher, R. L. & Bryan, W. B. (1984). Mineralogical variability of the uppermost mantle along mid-ocean ridges. *Earth and Planetary Science Letters* **69**, 88–106.
- Ellam, R. M. (1992). Lithospheric thickness as a control on basalt geochemistry. *Geology* **20**, 153–156.
- Falloon, T. J. & Danyushevsky, L. V. (2000). Melting of refractory mantle at 1.5, 2 and 2.5 GPa under anhydrous and H₂O-undersaturated conditions: Implications for the petrogenesis of high-Ca boninites and the influence of subduction components on mantle melting. *Journal of Petrology* **41**, 257–283.
- Falloon, T. J. & Green, D. H. (1987). Anhydrous partial melting of MORB pyrolite and other peridotite compositions at 10 k bar: Implications for the origin of MORB glasses. *Mineralogy and Petrology* **37**, 181–219.
- Falloon, T. J. & Green, D. H. (1988). Anhydrous partial melting of peridotite from 8 to 35 kb and the petrogenesis of MORB. *Journal of Petrology, Special Lithosphere Issue*, 379–414.
- Filiberto, J., Jackson, C., Le, L. & Treiman, A. H. (2009). Partitioning of Ni between olivine and an iron-rich basalt: Experiments, partition models, and planetary implications. *American Mineralogist* **94**, 256–261.
- Fischer, K. M., Ford, H. A., Abt, D. L. & Rychert, C. A. (2010). The lithosphere–asthenosphere boundary. *Annual Review of Earth and Planetary Sciences* **38**, 551–571.
- Foulger, G. R. (2005). Mantle plumes: Why the current skepticism? *Chinese Science Bulletin* **50**, 1555–1560.
- Foulger, G. R., Natland, J. H., Presnall, D. C. & Anderson, D. L. (eds) (2005). *Plates, Plumes, and Paradigms*. Geological Society of America, *Special Papers* **388**, 881 p.
- Gaetani, G. A. & Grove, T. L. (1998). The influence of water on melting of mantle peridotite. *Contributions to Mineralogy and Petrology* **131**, 323–346.
- Gao, S., Rudnick, R. L., Xu, W.-L., Yuan, H.-L., Liu, Y.-S., Walker, R. J., Igor, S., Puchtel, S., Liu, X., Huang, H., Wang, X.-R. & Yang, J. (2008). Recycling deep cratonic lithosphere and generation of intraplate magmatism in the North China Craton. *Earth and Planetary Science Letters* **270**, 41–53.
- Green, D. H. (1971). Composition of basaltic magmas as indicators of conditions of origin: Application to oceanic volcanism. *Philosophical Transaction of the Royal Society of London, Series A* **268**, 707–725.
- Green, D. H. (1973). Experimental studies on a modal upper mantle composition at high pressure under water-saturated and water-undersaturated conditions. *Earth and Planetary Science Letters* **19**, 37–53.
- Green, D. H. (1991). The Earth's lithosphere and asthenosphere—Concepts and constraints derived from petrology and high pressure experiments. In: Drummond, B. J. (ed.) *The Australian Lithosphere*, Geological Society of Australia *Special Publication* **17**, 1–22.
- Green, D. H. & Falloon, T. J. (1998). Pyrolite: A Ringwood concept and its current expression. In: Jackson, I. (ed.) *The Earth's Mantle, Composition, Structure, and Evolution*. Cambridge: Cambridge University Press, pp. 311–380.
- Green, D. H. & Falloon, T. J. (2005). Primary magmas at mid-ocean ridges, 'hotspots', and other intraplate settings: Constraints on mantle potential temperature. In: Foulger, G. R., Natland, J. H., Presnall, D. C. & Anderson, D.L. (eds) *Plates, Plumes, and Paradigms*. Geological Society of America, *Special Papers* **388**, 217–248.
- Green, D. H. & Liebermann, R. C. (1976). Phase equilibria and elastic properties of a Pyrolite model for the oceanic upper mantle. *Tectonophysics* **32**, 61–92.
- Green, D. H., Falloon, T. J., Eggins, S. M. & Yaxley, G. M. (2001). Primary magmas and mantle temperatures. *European Journal of Mineralogy* **13**, 437–451.

- Green, D. H., Hibberson, W. O., Kovacs, I. & Rosenthal, A. (2010). Water and its influence on the lithosphere–asthenosphere boundary. *Nature* **467**, 448–451.
- Haase, K. M. (1996). The relationship between the age of the lithosphere and the composition of oceanic magmas: constraints on partial melting, mantle sources and the thermal structure of the plates. *Earth and Planetary Science Letters* **144**, 75–92.
- Hart, S. R. & Davis, K. E. (1978). Nickel partitioning between olivine and silicate melt. *Earth and Planetary Science Letters* **40**, 203–219.
- Herzberg, C. (1992). Depth and degree of melting of komatiites. *Journal of Geophysical Research* **97**, 4521–4540.
- Herzberg, C. & Asimow, P. D. (2008). Petrology of some oceanic island basalts: PRIMELT2.XLS software for primary magma calculation. *Geochemistry, Geophysics, Geosystems* **9**, doi:10.1029/2008GC002057.
- Herzberg, C. & Gazel, E. (2009). Petrological evidence for secular cooling in mantle plumes. *Nature* **485**, 619–623.
- Herzberg, C. & O'Hara, M. J. (2002). Plume-associated ultramafic magmas of Phanerozoic age. *Journal of Petrology* **43**, 1857–1883.
- Herzberg, C. & Zhang, J. (1996). Melting experiments on anhydrous peridotite KLB-1: Compositions of magmas in the upper mantle and transition zone. *Journal of Geophysical Research* **101**, 8271–8295.
- Herzberg, C., Asimow, P. D., Arndt, N., Niu, Y. L., Leshner, C. M., Fitton, J. G., Cheadle, M. J. & Saunders, A. D. (2007). Temperatures in ambient mantle and plumes: Constraints from basalts, picrites and komatiites. *Geochemistry, Geophysics, Geosystems* **8**, doi:10.1029/2006GC001390.
- Hirano, N., Takahashi, E., Yamamoto, J., Abe, N., Ingle, S. P., Kaneoka, I., Hirata, T., Kimura, J.-I., Ishi, T., Ogawa, Y., Machida, S. & Suyehiro, K. (2006). Volcanism in response to plate flexure. *Science* **313**, 1426–1428.
- Hirose, K. & Kushiro, I. (1993). Partial melting of dry peridotites at high pressures: Determination of compositions of melts segregated from peridotite using aggregates of diamonds. *Earth and Planetary Science Letters* **114**, 477–489.
- Hirschmann, M. M. (2000). Mantle solidus: Experimental constraints and the effects of peridotite composition. *Geochemistry, Geophysics, Geosystems* **1**, doi:10.1029/2000GC000070.
- Hirschmann, M. M. & Stolper, E. M. (1996). A possible role for garnet pyroxenite in the origin of the 'garnet signature' in MORB. *Contributions to Mineralogy and Petrology* **124**, 185–208.
- Hofmann, A. W. (1997). Mantle geochemistry: The message from oceanic volcanism. *Nature* **385**, 219–229.
- Huang, J. & Zhong, S. (2005). Sublithospheric small-scale convection and its implications for the residual topography at old ocean basins and the plate model. *Journal of Geophysical Research* **110**, B05404, doi:10.1029/2004JB003153.
- Humayun, M., Qin, L. & Norman, M. D. (2004). Geochemical evidence for excess iron in the mantle beneath Hawaii. *Science* **306**, 91–94.
- Humphreys, E. R. & Niu, Y. L. (2009). On the composition of ocean island basalts (OIB): The effects of lithospheric thickness variation and mantle metasomatism. *Lithos* **112**, 118–136.
- Jaques, A. L. & Green, D. H. (1980). Anhydrous melting of peridotite at 0–15 kb pressure and the genesis of tholeiitic basalts. *Contributions to Mineralogy and Petrology* **73**, 287–310.
- Julian, B. R. (2005). What can seismology say about hotspots? In: Foulger, G. R., Natland, J. H., Presnall, D. C. & Anderson, D. L. (eds) *Plates, Plumes and Paradigms. Geological Society of America Special Paper* **388**, 155–170.
- Kawakatsu, H., Kumar, P., Takei, Y., Shinohara, M., Kanazawa, T., Araki, E. & Suyehiro, K. (2009). Seismic evidence for sharp lithosphere–asthenosphere boundaries of oceanic plates. *Science* **324**, 449–502.
- Kinzler, R. J. & Grove, T. L. (1992). Primary magmas of mid-ocean ridge basalts, 2, applications. *Journal of Geophysical Research* **97**, 6907–6926.
- Klein, E. M. & Langmuir, C. H. (1987). Global correlations of ocean ridge basalt chemistry with axial depth and crustal thickness. *Journal of Geophysical Research* **92**, 8089–8115.
- Kumar, P. & Kawakatsu, H. (2011). Imaging the seismic lithosphere–asthenosphere boundary of the oceanic plate. *Geochemistry, Geophysics, Geosystems* **12**, Q01006, doi:10.1029/2010GC003358.
- Lambert, I. B. & Wyllie, P. J. (1968). Stability of hornblende and a model for the low velocity zone. *Nature* **219**, 1240–1241.
- Lambert, I. B. & Wyllie, P. J. (1970). Low-velocity zone of the Earth's mantle—incipient melting caused by water. *Science* **169**, 764–766.
- Langmuir, C. H., Bender, J. F. & Batiza, R. (1986). Petrological and tectonic segmentation of the East Pacific Rise, 5°30'–14°30'N. *Nature* **332**, 422–429.
- Langmuir, C. H., Klein, E. M. & Plank, T. (1992). Petrological systematics of mid-ocean ridge basalts: Constraints on melt generation beneath ocean ridges. In: Phipps Morgan, J., Blackman, D. K. & Sinton, J. M. (eds) *Mantle Flow and Melt Generation at Mid-ocean Ridges. American Geophysical Union Monograph* **71**, 183–280.
- Lee, C.-T., Luffi, P., Plank, T., Dalton, H. & Leeman, W. P. (2009). Constraints on the depths and temperatures of basaltic magma generation on Earth and other terrestrial planets using new thermobarometers for mafic magmas. *Earth and Planetary Science Letters* **279**, 20–33.
- Lee, W. J. & Wyllie, P. J. (2000). The system CaO–MgO–SiO₂–CO₂ at 1 GPa, metasomatic wehrlites, and primary carbonatite magmas. *Contributions to Mineralogy and Petrology* **138**, 214–228.
- Lee, W. J., Huang, W. L. & Wyllie, P. J. (2000). Melts in the mantle modeled in the system CaO–MgO–SiO₂–CO₂ at 2.7 GPa. *Contributions to Mineralogy and Petrology* **138**, 199–213.
- Li, C. & Ripley, E. M. (2008). Recycled crust in the mantle: Is high-Ni olivine the smoking gun or a red herring? *EOS Transactions, American Geophysical Union* **89**, Fall Meeting Supplement, Abstract V42B-07.
- Li, C. & Ripley, M. (2010). The relative effects of composition and temperature on olivine–liquid Ni partitioning: Statistical deconvolution and implications for petrologic modelling. *Chemical Geology* **275**, 99–104.
- Liu, Y., Gao, S., Kelemen, P. B. & Xu, W. (2008). Recycled crust controls contrasting source compositions of Mesozoic and Cenozoic basalts in the North China Craton. *Geochimica et Cosmochimica Acta* **72**, 2349–2376.
- Mahoney, J. J., Sinton, J. M., Kurz, D. M., Macdougall, J. D., Spencer, K. J. & Lugmair, G. W. (1994). Isotope and trace element characteristics of a super-fast spreading ridge: East Pacific Rise, 13–23°S. *Earth and Planetary Science Letters* **121**, 173–193.
- Matzen, A. K., Baker, M. B., Beckett, J. R. & Stolper, E. M. (2009). The temperature and pressure dependence of Ni partitioning between olivine and MgO-rich silicate melt. *Geochimica et Cosmochimica Acta* **73**, A851–A851.
- McDonough, W. F. & Sun, S.-s. (1995). The composition of the Earth. *Chemical Geology* **120**, 223–253.
- McKenzie, D. & Bickle, M. J. (1988). The volume and composition of melt generated by extension of the lithosphere. *Journal of Petrology* **29**, 625–679.
- McKenzie, D. P., Jackson, J. & Priestley, K. (2005). Thermal structure of oceanic and continental lithosphere. *Earth and Planetary Science Letters* **233**, 337–349.

- Millhollen, G. L., Irving, A. J. & Wyllie, P. J. (1974). Melting interval of peridotite with 5.7 per cent water to 30 kilobars. *Journal of Geology* **82**, 575–587.
- Morgan, W. J. (1971). Convection plumes in the lower mantle. *Nature* **230**, 42–43.
- Morgan, W. J. (1972). Plate motions and deep mantle convection. In: Shagam, R., Hargraves, R. B., Morgan, W. J., Van Houten, F. B., Burk, C. A., Holland, H. D. & Hollister, L. C. (eds) *Studies in Earth and Space Sciences, Geological Society of America, Memoirs* **132**, 7–22.
- Mysen, B. O. & Kushiro, I. (1979). Pressure dependence of nickel partitioning between forsterite and aluminous silicate melts. *Earth and Planetary Science Letters* **42**, 383–388.
- Niu, Y. L. (1997). Mantle melting and melt extraction processes beneath ocean ridges: Evidence from abyssal peridotites. *Journal of Petrology* **38**, 1047–1074.
- Niu, Y. L. (2004). Bulk rock major and trace element compositions of abyssal peridotites: Implications for mantle melting, melt extraction and post-melting processes beneath ocean ridges. *Journal of Petrology* **45**, 2423–2458.
- Niu, Y. L. (2005). On the great mantle plume debate. *Chinese Science Bulletin* **50**, 1537–1540.
- Niu, Y. L. (2009). Some basic concepts and problems on the petrogenesis of intra-plate ocean island basalts (OIB). *Chinese Science Bulletin* **54**, 4148–4160.
- Niu, Y. L. & Batiza, R. (1991). An empirical method for calculating melt compositions produced beneath mid-ocean ridges: Application for axis and off-axis (seamounts) melting. *Journal of Geophysical Research* **96**, 21753–21777.
- Niu, Y. L. & Batiza, R. (1997). Trace element evidence from seamounts for recycled oceanic crust in the eastern Pacific mantle. *Earth and Planetary Science Letters* **148**, 471–483.
- Niu, Y. L. & Hékinian, R. (1997a). Spreading rate dependence of the extent of mantle melting beneath ocean ridges. *Nature* **385**, 326–329.
- Niu, Y. L. & Hékinian, R. (1997b). Basaltic liquids and harzburgitic residues in the Garrett Transform: A case study at fast-spreading ridges. *Earth and Planetary Science Letters* **146**, 243–258.
- Niu, Y. L. & O'Hara, M. J. (2003). Origin of ocean island basalts: A new perspective from petrology, geochemistry and mineral physics considerations. *Journal of Geophysical Research* **108**, 2209, doi:10.1029/2002JB002048.
- Niu, Y. L. & O'Hara, M. J. (2007). Varying Ni in OIB olivines—product of process not source. *Geochimica et Cosmochimica Acta* **71**, A721–A721.
- Niu, Y. L. & O'Hara, M. J. (2008). Global correlations of ocean ridge basalt chemistry with axial depth: A new perspective. *Journal of Petrology* **49**, 633–664.
- Niu, Y. L. & O'Hara, M. J. (2009). MORB mantle hosts the missing Eu (Sr, Nb, Ta and Ti) in the continental crust: New perspectives on crustal growth, crust–mantle differentiation and chemical structure of oceanic upper mantle. *Lithos* **112**, 1–17.
- Niu, Y. L., Waggoner, D. G., Sinton, J. M. & Mahoney, J. J. (1996). Mantle source heterogeneity and melting processes beneath sea-floor spreading centers: The East Pacific Rise, 18°–19°S. *Journal of Geophysical Research* **101**, 27711–27733.
- Niu, Y. L., Collerson, K. D., Batiza, R., Wendt, J. I. & Regelous, M. (1999). The origin of E-type MORB at ridges far from mantle plumes: The East Pacific Rise at 11°20'. *Journal of Geophysical Research* **104**, 7067–7087.
- Niu, Y. L., Bideau, D., Hékinian, R. & Batiza, R. (2001). Mantle compositional control on the extent of mantle melting, crust production, gravity anomaly, ridge morphology, and ridge segmentation: A case study at the Mid-Atlantic Ridge 33–35°N. *Earth and Planetary Science Letters* **286**, 383–399.
- Niu, Y. L., Regelous, M., Wendt, J. I., Batiza, R. & O'Hara, M. J. (2002). Geochemistry of near-EPR seamounts: Importance of source vs process and the origin of enriched mantle component. *Earth and Planetary Science Letters* **199**, 327–345.
- Niu, Y. L., Wilson, M., Humphreys, E. R. & O'Hara, M. J. (2010). On the origin of OIB: Processes, sources and mantle convection. *Geochimica et Cosmochimica Acta* **74**, A763–A763.
- O'Hara, M. J. (1968). Are ocean floor basalts primary magmas? *Nature* **220**, 683–686.
- O'Hara, M. J. (1977). Geochemical evolution during fractional crystallisation of a periodically refilled magma chamber. *Nature* **266**, 503–507.
- Park, K.-H. (1990). Sr, Nd and Pb isotope studies of ocean island basalts: Constraints on their origin and evolution, PhD thesis, Columbia University, New York.
- Parman, S. W. & Grove, T. L. (2004). Harzburgite melting with and without H₂O: Experimental data and predictive modelling. *Journal of Geophysical Research* **109**, B02201, doi:10.1029/2003JB002566.
- Parson, B. & McKenzie, D. (1978). Mantle convection and thermal structure of plates. *Journal of Geophysical Research* **83**, 4485–4496.
- Parsons, B. & Sclater, J. G. (1977). An analysis of the variation of ocean floor bathymetry and heat flow with age. *Journal of Geophysical Research* **82**, 803–827.
- Phipps Morgan, J. & Smith, W. H. F. (1992). Flattening of the sea-floor depth–age curve as a response to asthenospheric flow. *Nature* **359**, 524–527.
- Presnall, D. C. & Gudfinnsson, G. H. (2008). Origin of oceanic lithosphere. *Journal of Petrology* **49**, 615–632.
- Presnall, D. C. & Gudfinnsson, G. H. (2011). Oceanic volcanism from the low-velocity zone—geodynamic implications. *Journal of Petrology* **52**, 000–000.
- Putirka, K. D. (1999). Melting depths and mantle heterogeneity beneath Hawaii and the East Pacific Rise: Constraints from Na/Ti and rare earth element ratios. *Journal of Geophysical Research* **104**, 2817–2829.
- Putirka, K. D. (2005). Mantle potential temperatures at Hawaii, Iceland, and the mid-ocean ridge system, as inferred from olivine phenocrysts: Evidence for thermally driven mantle plumes. *Geochemistry, Geophysics, Geosystems* **6**, Q05L08, doi:10.1029/2005GC000915.
- Putirka, K. D. (2008a). Excess temperatures at ocean islands. Implications for mantle layering and convection. *Geology* **36**, 283–286.
- Putirka, K. D. (2008b). Thermometers and barometers for volcanic systems. In: Putirka, K. D. & Tepley, F. J., III (eds) *Minerals, Inclusions and Volcanic Processes. Mineralogical Society of America and Geochemical Society, Reviews in Mineralogy and Geochemistry* **69**, 61–120.
- Putirka, K. D., Ryerson, F. J., Perfit, M. & Ridley, W. I. (2011). Mineralogy and composition of oceanic mantle. *Journal of Petrology* **52**, 279–313.
- Rychert, C. A. & Shearer, P. M. (2009). A global view of the lithosphere–asthenosphere boundary. *Science* **324**, 495–498.
- Salters, V. J. M. & Hart, S. R. (1989). The hafnium paradox and the role of garnet in the source of mid-ocean ridge basalts. *Nature* **342**, 420–422.
- Seifert, S., O'Neill, H. St. C. & Brey, G. (1988). The partitioning of Fe, Ni, and Co between olivine, metal, and basaltic liquid: An experimental and thermodynamic investigation, with implication to the composition of the lunar core. *Geochimica et Cosmochimica Acta* **52**, 603–616.

- Sinton, J. M., Smaglik, S. M. & Mahoney, J. J. (1991). Magmatic processes at superfast spreading mid-ocean ridges: Glass compositional variations along the East Pacific Rise 13°–23°S. *Journal of Geophysical Research* **96**, 6133–6155.
- Sleep, N. H. (1987). Lithospheric heating by mantle plumes. *Journal of Geophysical Research* **95**, 6715–6736.
- Sleep, N. H. (2011). Small-scale convection beneath oceans and continents. *Chinese Science Bulletin* **56**, 1292–1320.
- Sobolev, A. V., Hofmann, A. W., Sobolev, S. V. & Nikogosian, I. K. (2005). A olivine-free mantle source of Hawaii shield basalts. *Nature* **434**, 590–597.
- Sobolev, A. V., Hofmann, A. W., Kuzmin, D. V. *et al.* (2007). The amount of recycled crust in sources of mantle-derived melts. *Science* **316**, 412–417.
- Stein, C. A. & Stein, S. (1992). A model for the global variation in oceanic depth and heat-flow with lithospheric age. *Nature* **359**, 123–129.
- Stolper, E. (1980). A phase diagram for mid-ocean ridge basalts: Preliminary results and implications for petrogenesis. *Contributions to Mineralogy and Petrology* **74**, 13–27.
- Sun, S.-s. & McDonough, W. F. (1989). Chemical and isotopic systematics in ocean basalt: Implication for mantle composition and processes. In: Saunders, A. D. & Norry, M. J. (eds) *Magmatism in the Ocean Basins*. Geological Society, London, *Special Publications* **42**, 313–345.
- Takahashi, E. & Kushiro, I. (1983). Melting of a dry peridotite at high pressures and basaltic magma genesis. *American Mineralogist* **68**, 859–879.
- Taura, H., Yurimoto, H., Kurita, K. & Sueno, S. (1998). Pressure dependence on partition coefficients for trace elements between olivine and the coexisting melts. *Physics and Chemistry of Minerals* **25**, 469–484.
- Walker, D., Shibata, T. & DeLong, S. E. (1979). Abyssal tholeiites from the Oceanographer Fracture Zone, II, Phase equilibria and mixing. *Contributions to Mineralogy and Petrology* **70**, 111–125.
- Walter, M. J. (1998). Melting of garnet peridotite and the origin of komatiite and depleted lithosphere. *Journal of Petrology* **39**, 29–60.
- Wang, Z. R. & Gaetani, G. A. (2008). Partitioning of Ni between olivine and siliceous eclogite partial melt: experimental constraints on the mantle source of Hawaiian basalts. *Contributions to Mineralogy and Petrology* **156**, 661–678.
- Wessel, P. (1997). Sizes and ages of seamounts using remote sensing: Implications for intraplate volcanism. *Science* **277**, 802–805.
- White, B. S. & Wyllie, P. J. (1992). Phase relations in synthetic lherzolite–H₂O–CO₂ from 20–30 kb, with applications to melting and metasomatism. *Journal of Volcanology and Geothermal Research* **50**, 117–130.
- Wilson, J. T. (1963a). A possible origin of the Hawaiian Islands. *Canadian Journal of Physics* **41**, 863–870.
- Wilson, J. T. (1963b). Evidence from islands on the spreading of the ocean floor. *Nature* **197**, 536–538.
- Wood, B. J. & Yuen, D. A. (1983). The role of lithosphere phase transitions on seafloor flattening at old ages. *Earth and Planetary Science Letters* **66**, 303–314.
- Wyllie, P. J. (1978). Mantle fluid compositions buffered in peridotite–CO₂–H₂O by carbonates, amphibole, and phlogopite. *Journal of Geology* **86**, 687–713.
- Wyllie, P. J. (1987). Discussion of recent papers on carbonated peridotite, bearing on mantle metasomatism and magmatism. *Earth and Planetary Science Letters* **82**, 391–397, 401–402.
- Wyllie, P. J. (1988a). Solidus curves, mantle plumes, and magma generation beneath Hawaii. *Journal of Geophysical Research* **93**, 4171–4181.
- Wyllie, P. J. (1988b). Magma genesis, plate tectonics, and chemical differentiation of the Earth. *Reviews of Geophysics* **26**, 370–404.
- Wyllie, P. J. & Huang, W. L. (1975). Influence of mantle CO₂ in the generation of carbonatites and kimberlites. *Nature* **257**, 297–299.
- Wyllie, P. J. & Ryabchikov, I. D. (2000). Volatile components, magmas, and critical fluids in upwelling mantle. *Journal of Petrology* **41**, 1195–1206.
- Wyllie, P. J., Huang, W.-L., Otto, J. & Byrnes, A. P. (1983). Carbonation of peridotites and decarbonation of siliceous dolomites represented in the system CaO–MgO–SiO₂–CO₂ to 30 kbar. *Tectonophysics* **100**, 359–388.
- Yuen, D. A. & Fleitout, L. (1985). Thinning of the lithosphere by small scale convective destabilization. *Nature* **313**, 125–128.
- Zhang, J.-J., Zheng, Y.-F. & Zhao, Z.-F. (2009). Geochemical evidence for interaction between oceanic crust and lithospheric mantle in the origin of Cenozoic continental basalts in east–central China. *Lithos* **110**, 305–326.
- Zindler, A. & Hart, S. R. (1986). Chemical geodynamics. *Annual Review of Earth and Planetary Sciences* **14**, 493–571.
- Zindler, A., Staudigel, H. & Batiza, R. (1984). Isotope and trace element geochemistry of young Pacific seamounts: implications for the scale of mantle heterogeneity. *Earth and Planetary Science Letters* **70**, 175–195.
- Zou, H. (2000). Modeling of trace element fractionation during non-modal dynamic melting with linear variations in mineral/melt distribution coefficients. *Geochimica et Cosmochimica Acta* **64**, 1095–1102.